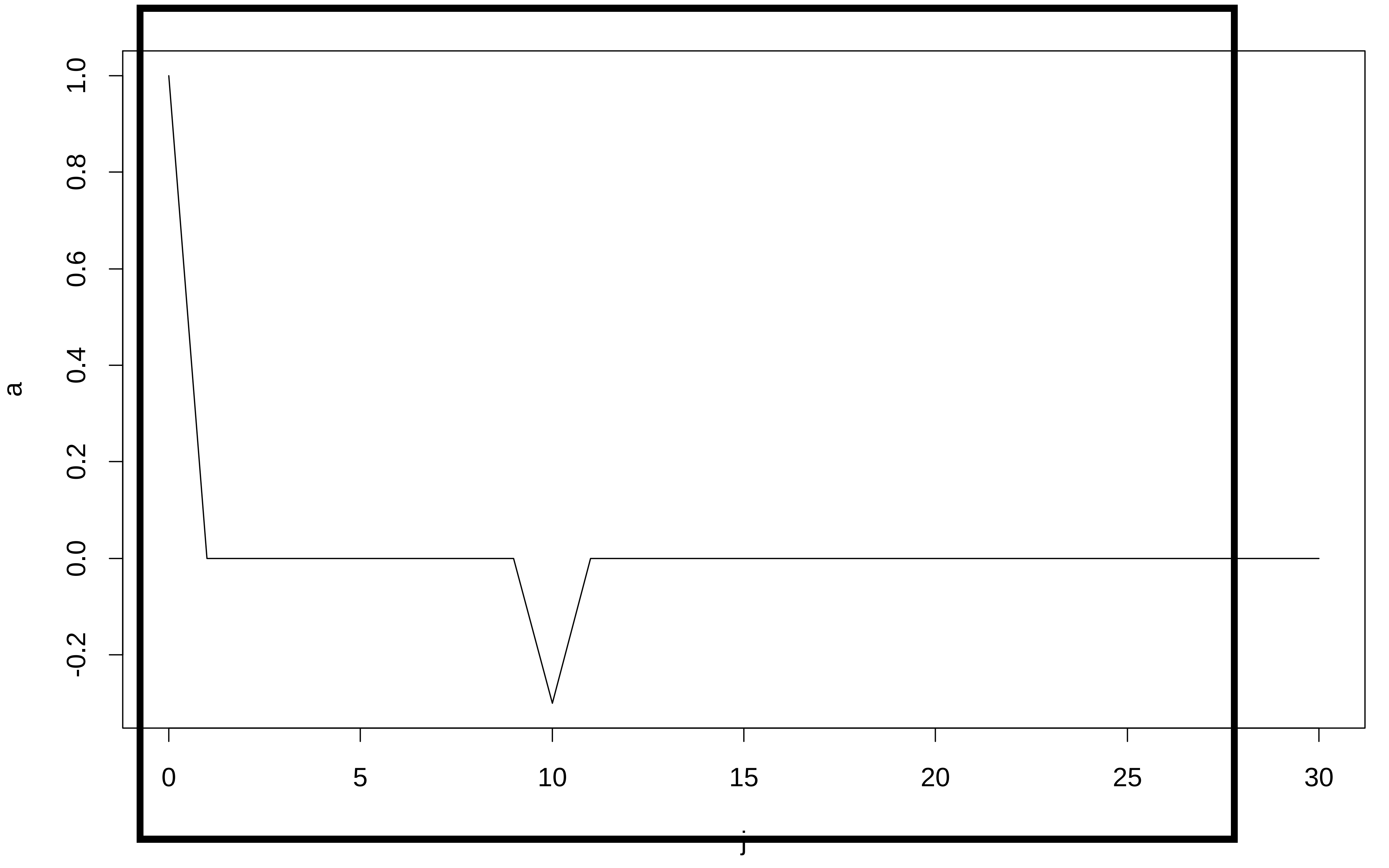

Figure 1: Hypothetical pulse sequence of a nuclear explosion or earthquake.

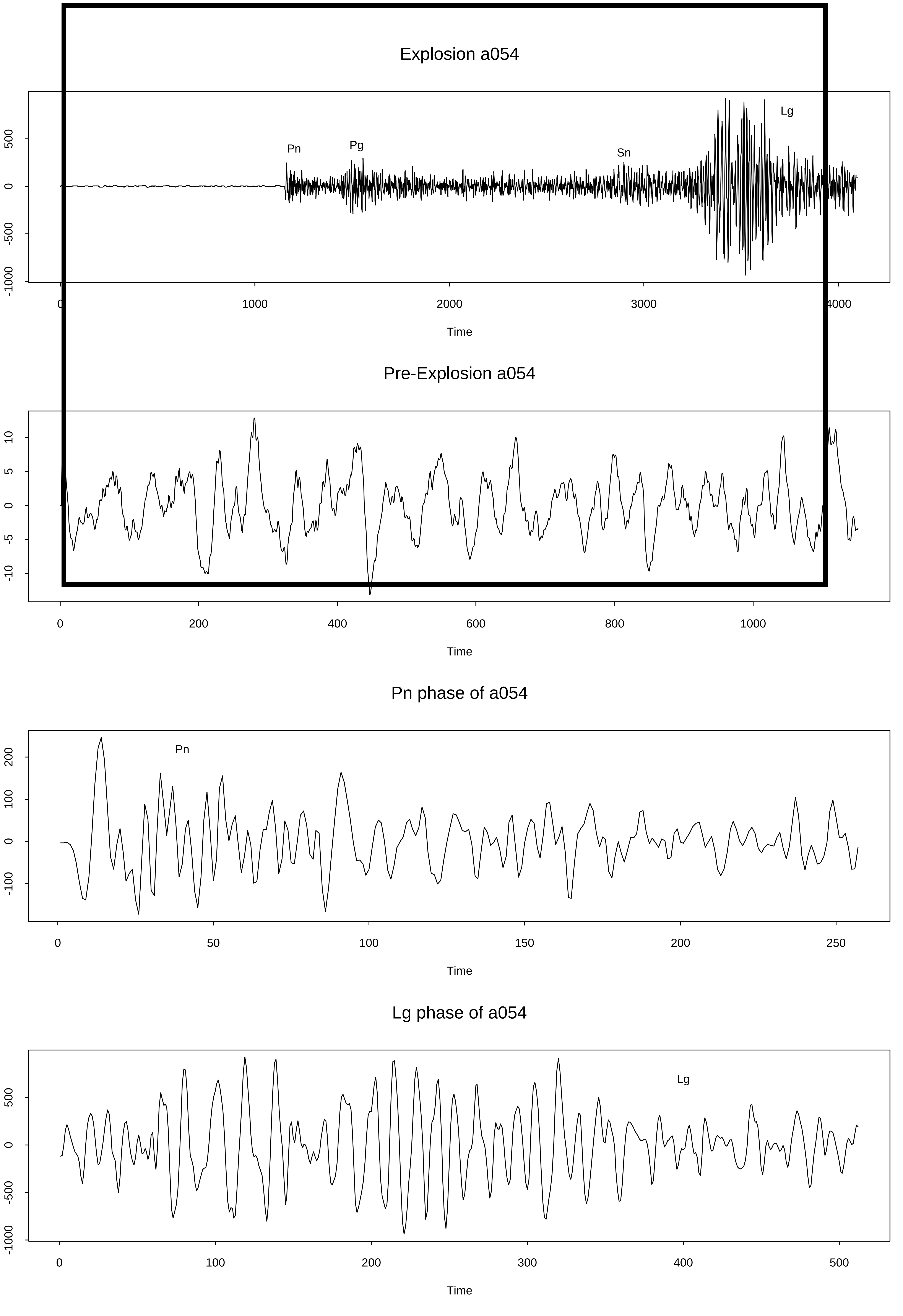

Figure 2: First panel (top): A seismogram of Event 054, a known ripple-fired mining explosion. Second panel: Enlargement of the pre-P_n noise. Third panel: Enlargement of the P_n-phase. Fourth panel: Enlargement of the L_g-phase.

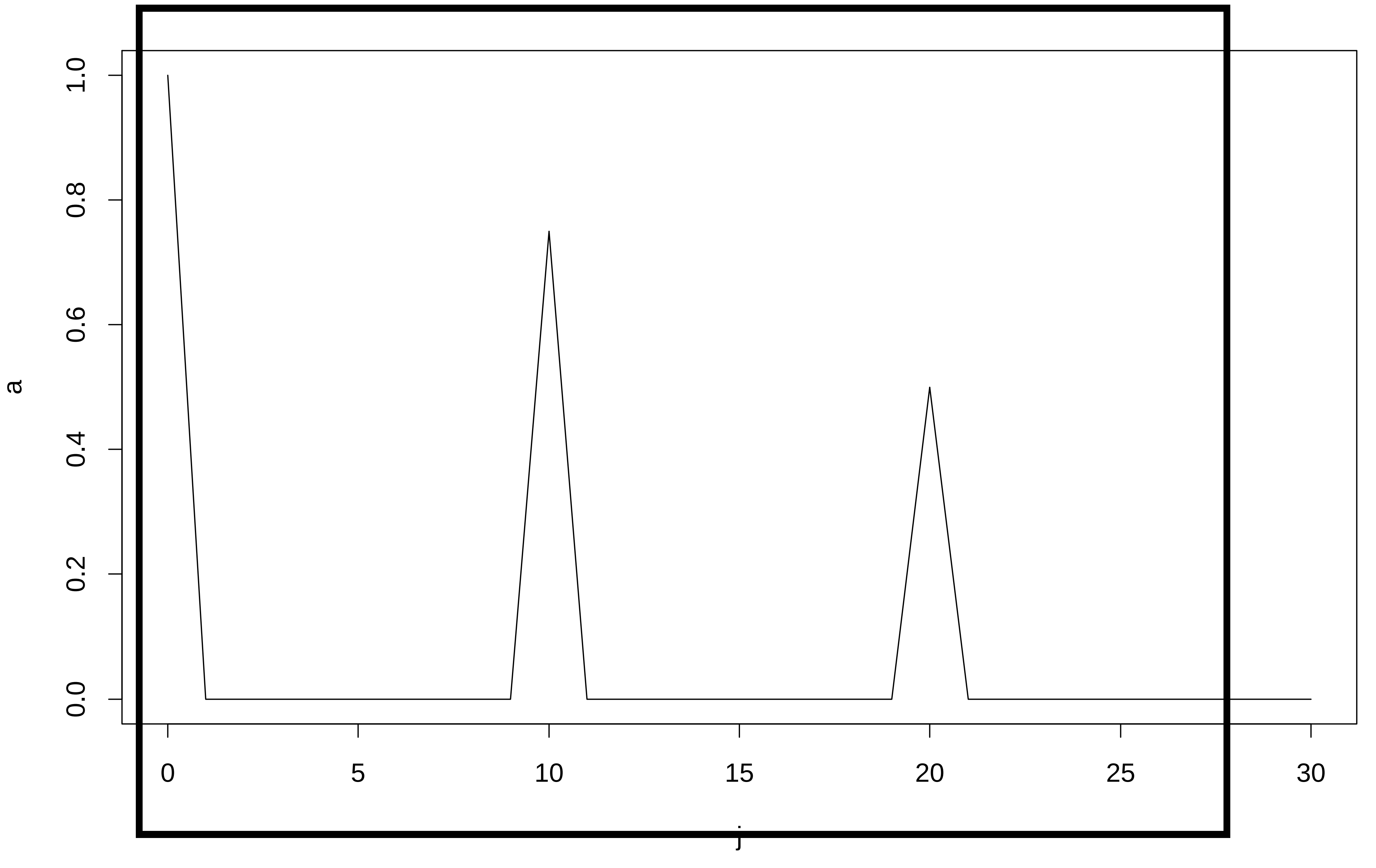

Figure 3: Hypothetical pulse sequence of a ripple-fired seismic event.

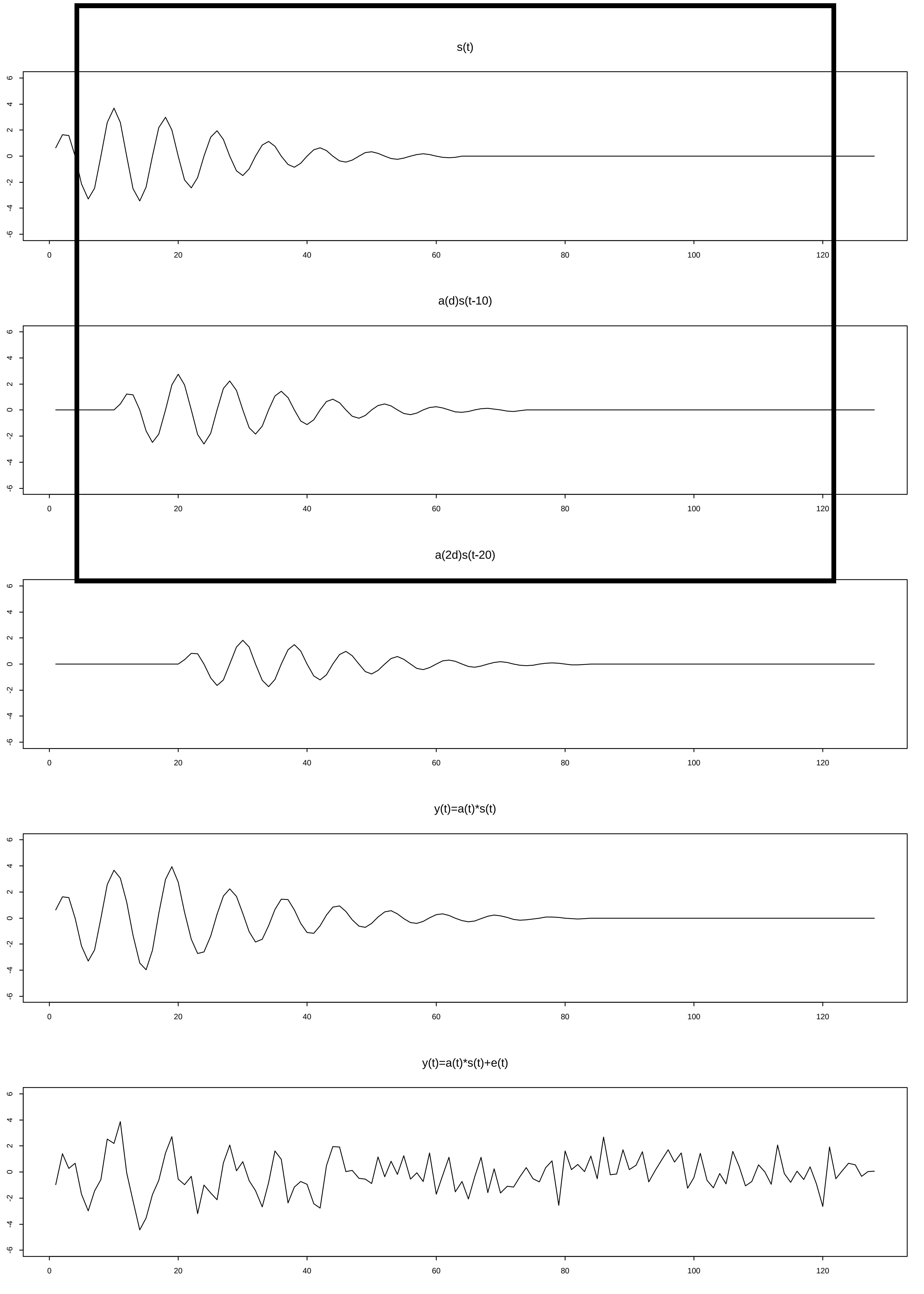

Figure 4: A convolution example.

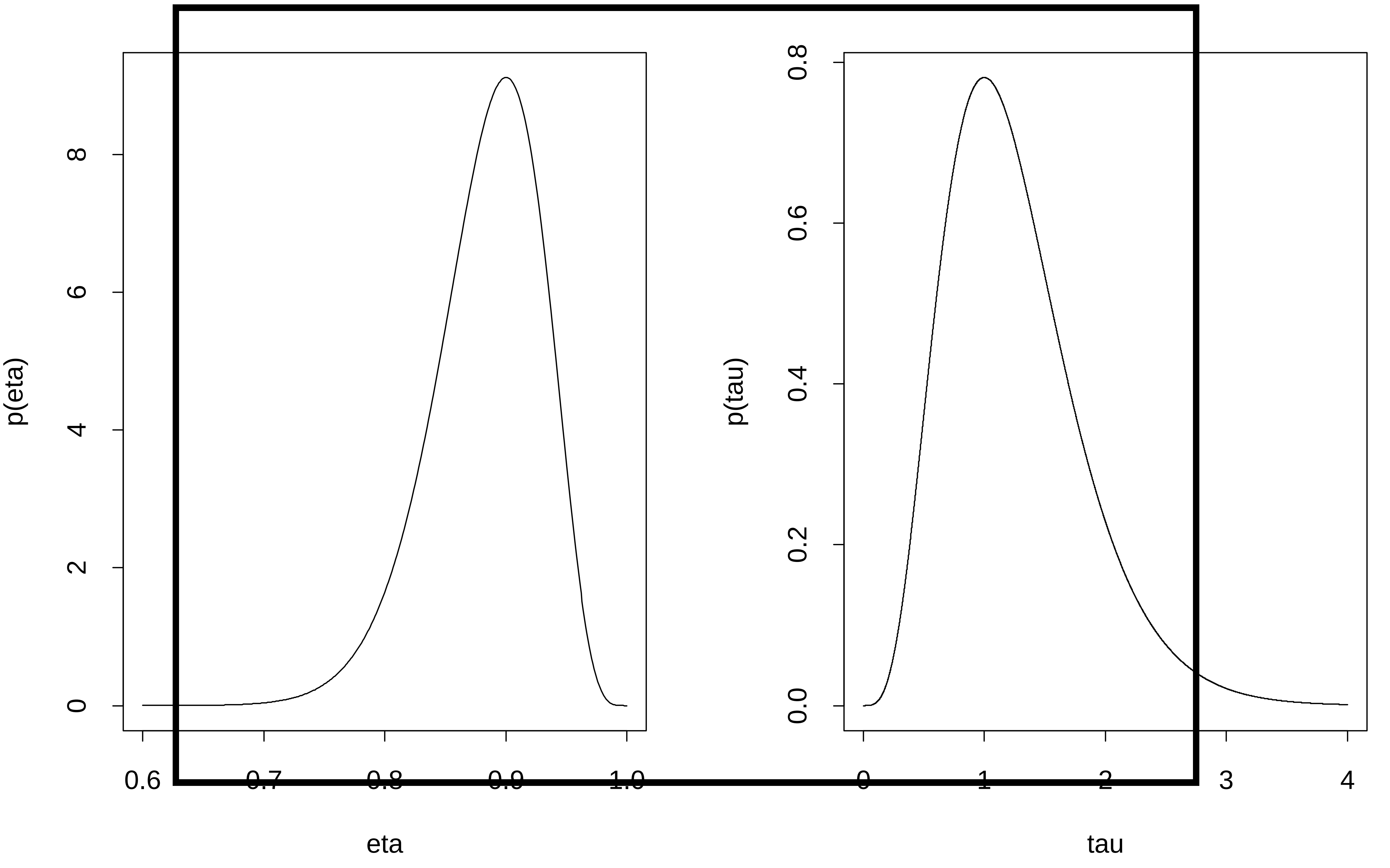

Figure 5: $\eta \sim$ Beta(43,5.67) and $\tau \sim$ Gamma(5,4).

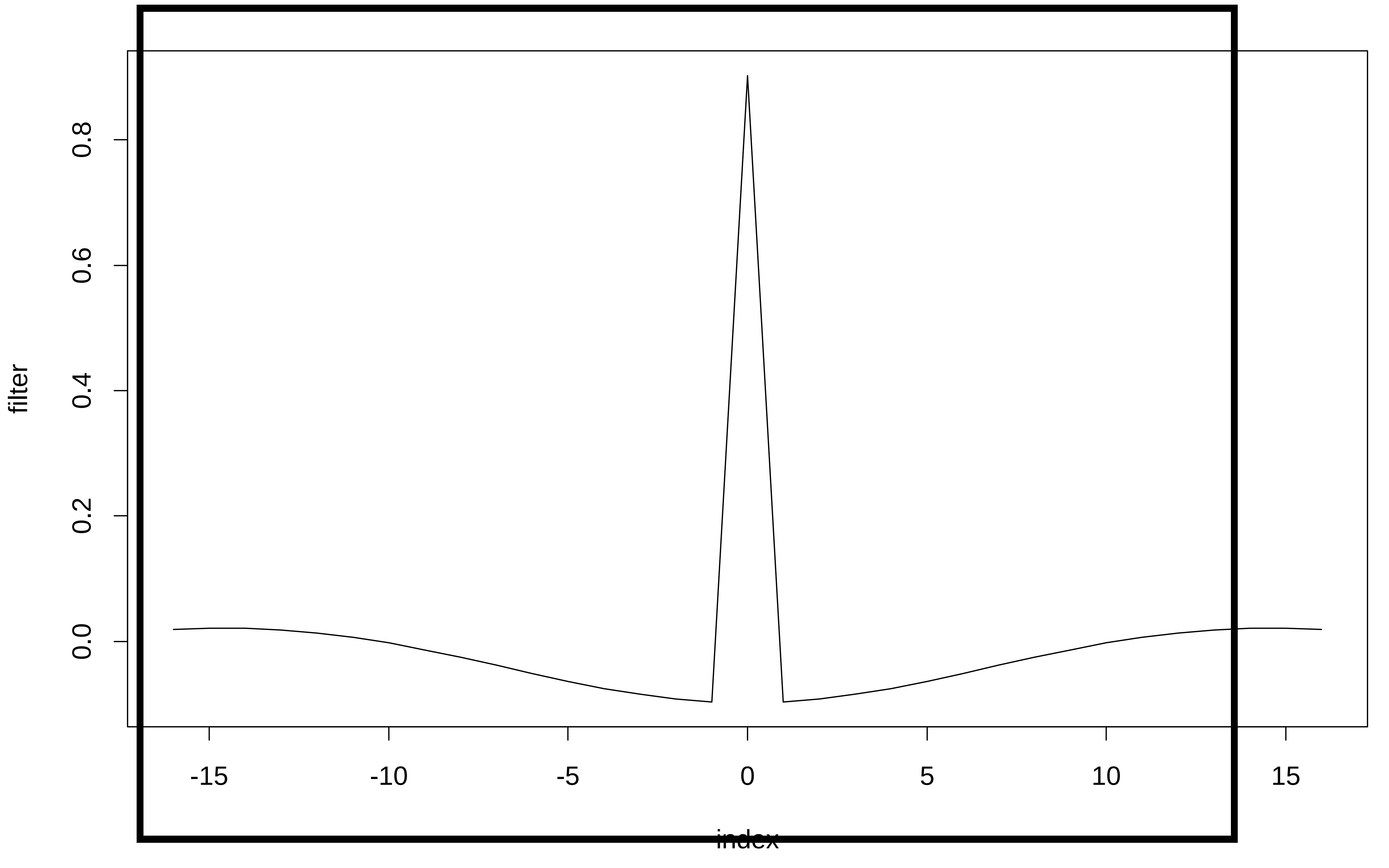

Figure 6: 32-point filter.

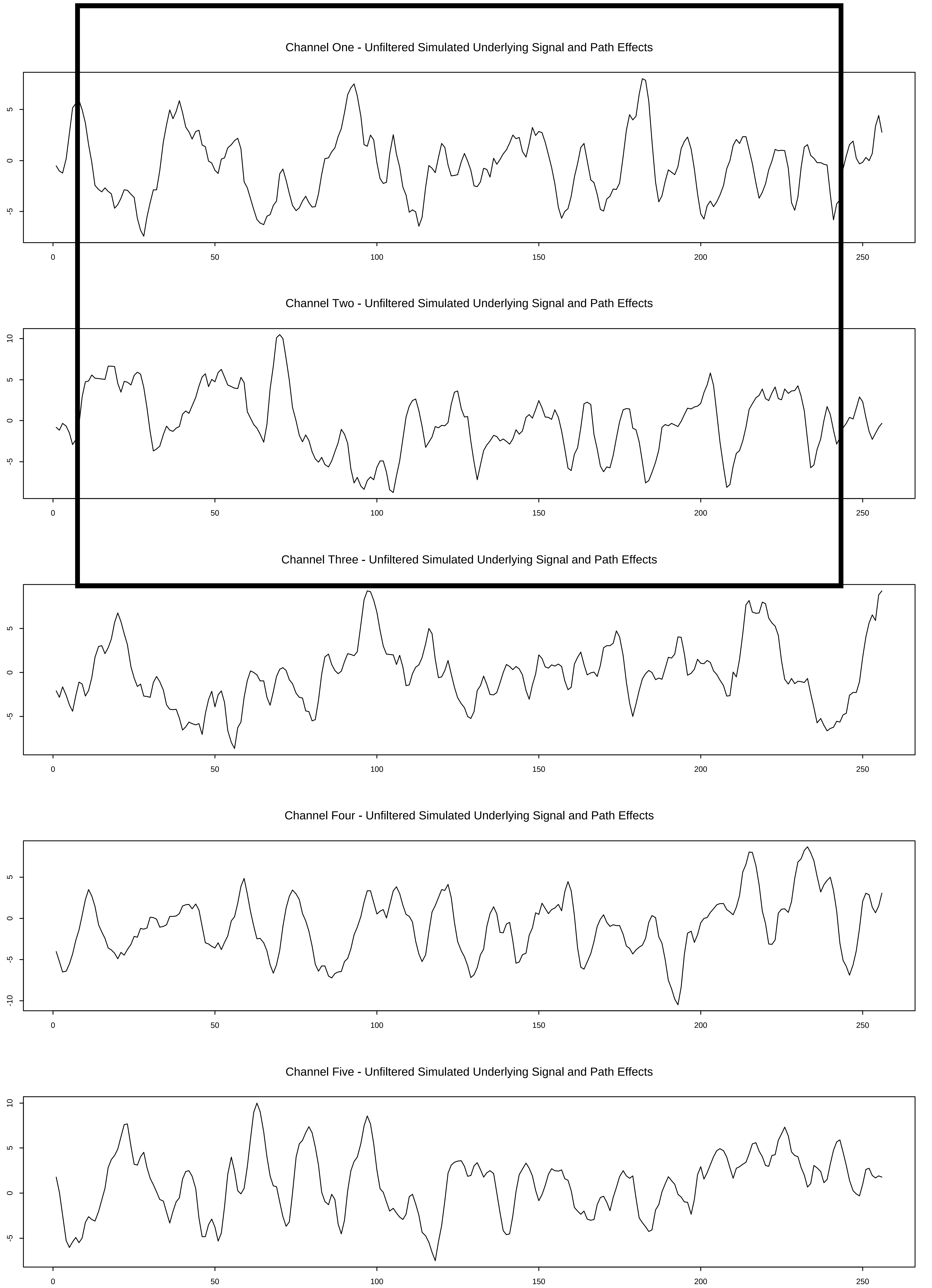

Figure 7: Unfiltered simulated underlying signals.

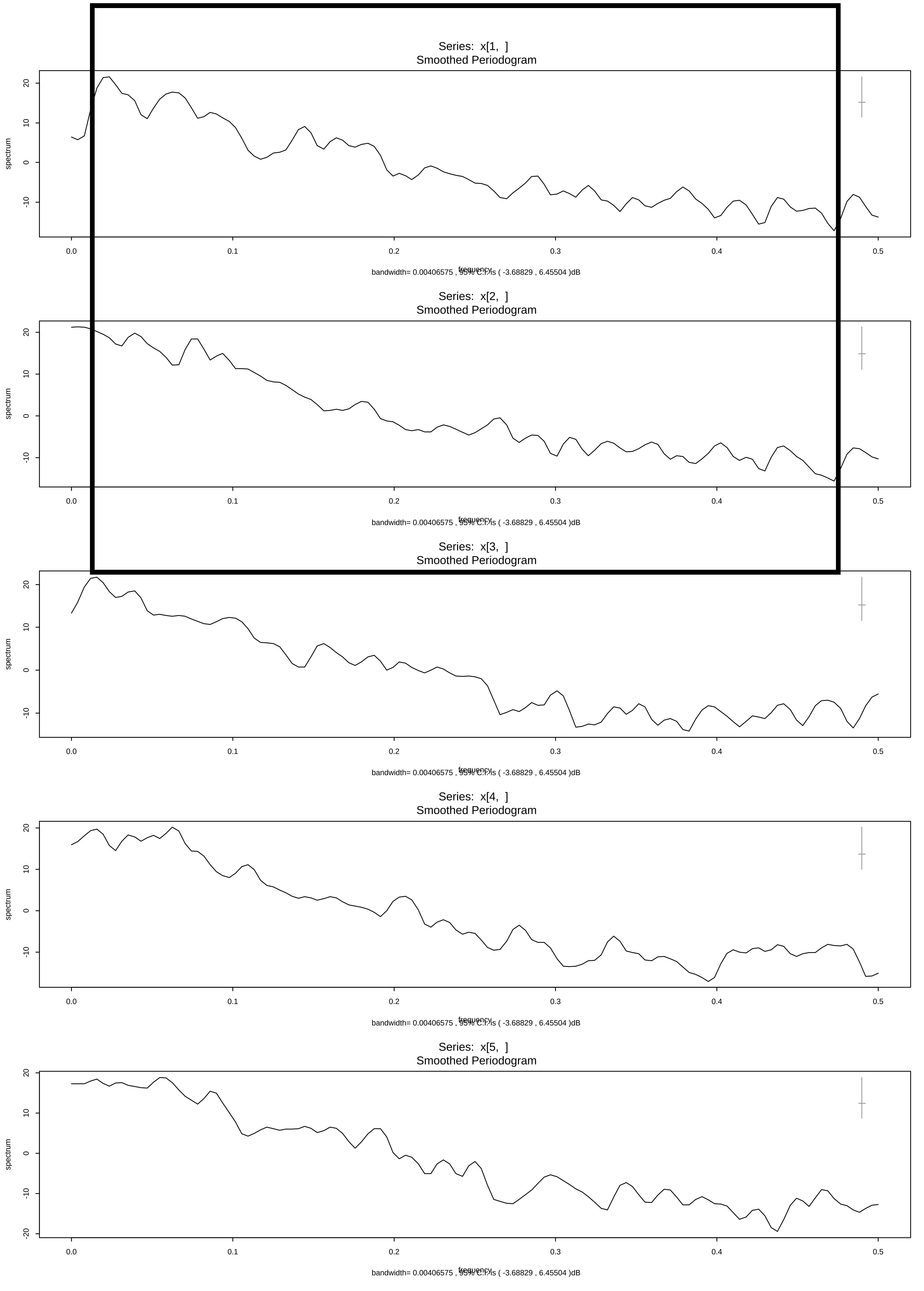

Figure 8: Spectra of the unfiltered simulated underlying signals.

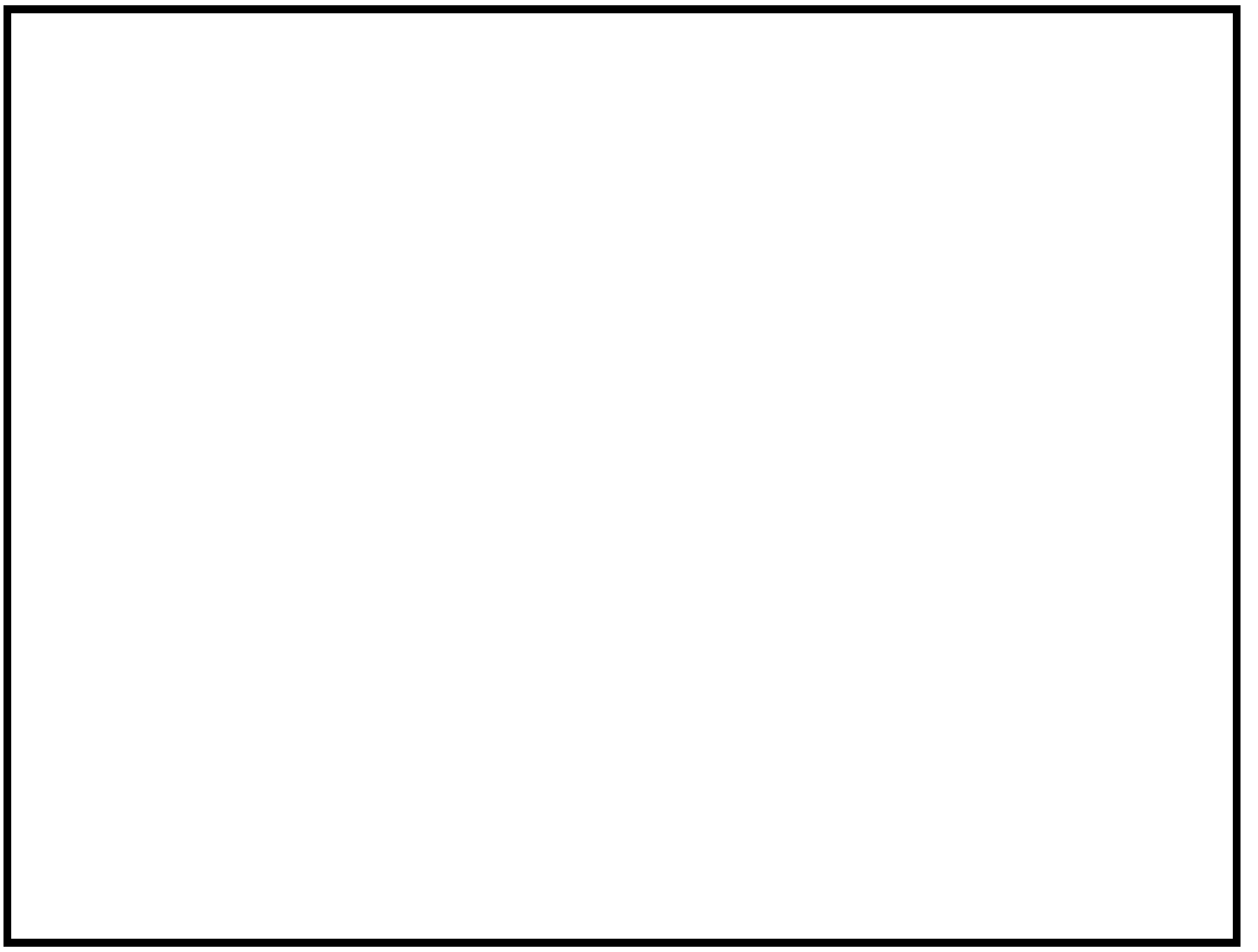

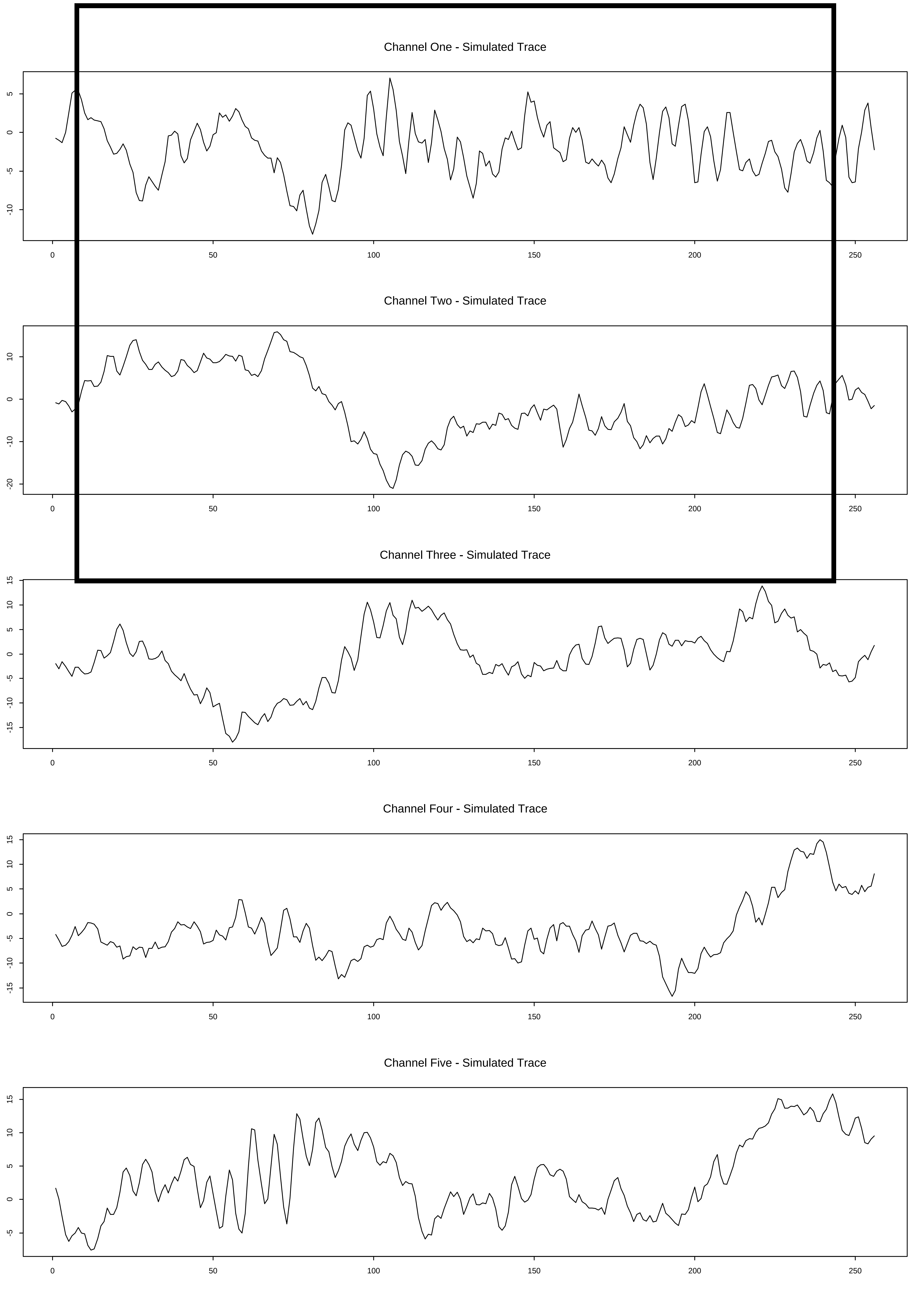

Figure 9: Simulated ripple-fired data traces, using unfiltered signals. Note that low frequencies are contained in these series.

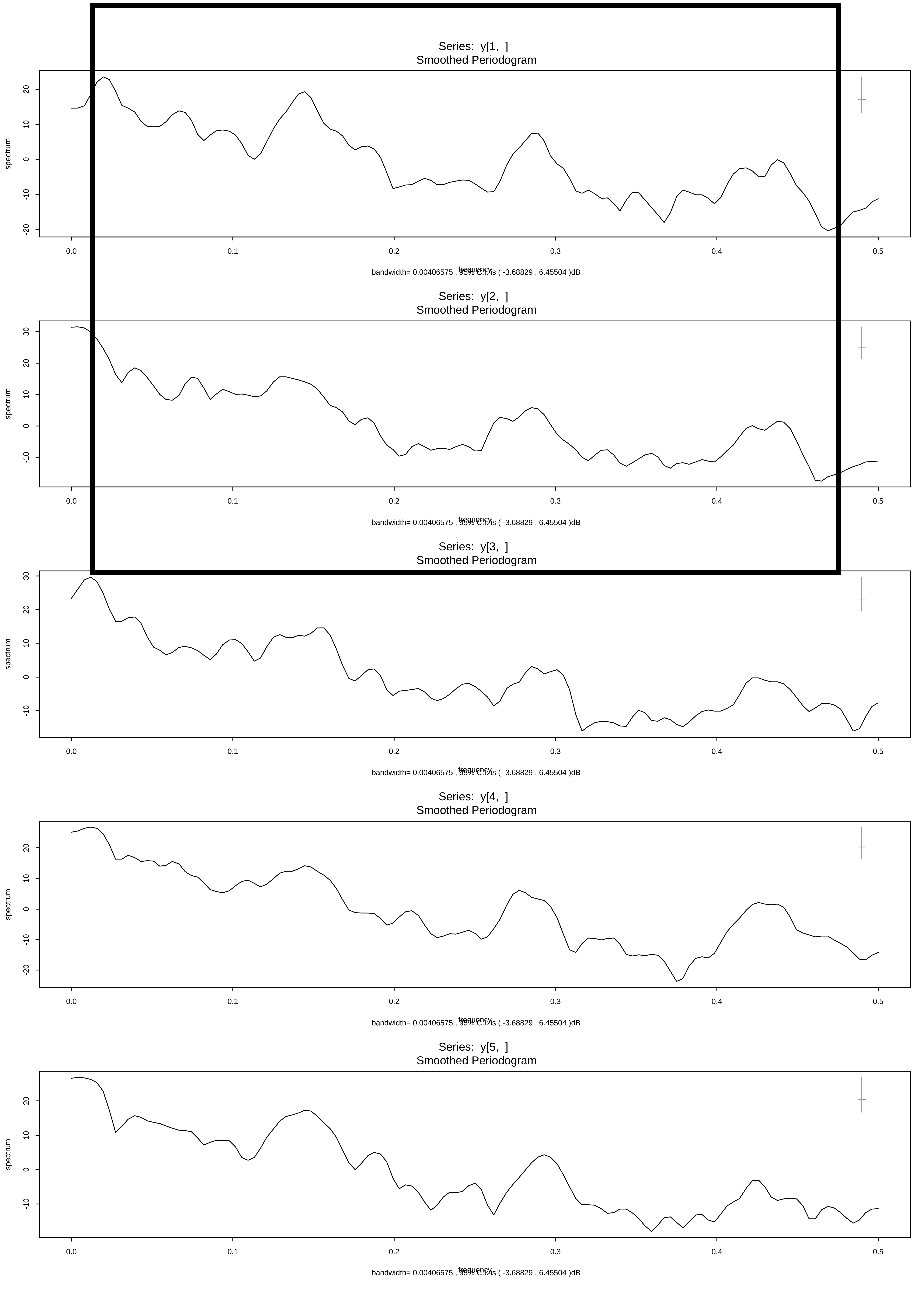

Figure 10: Spectra of the simulated ripple-fired traces. Note modulation in the spectra.

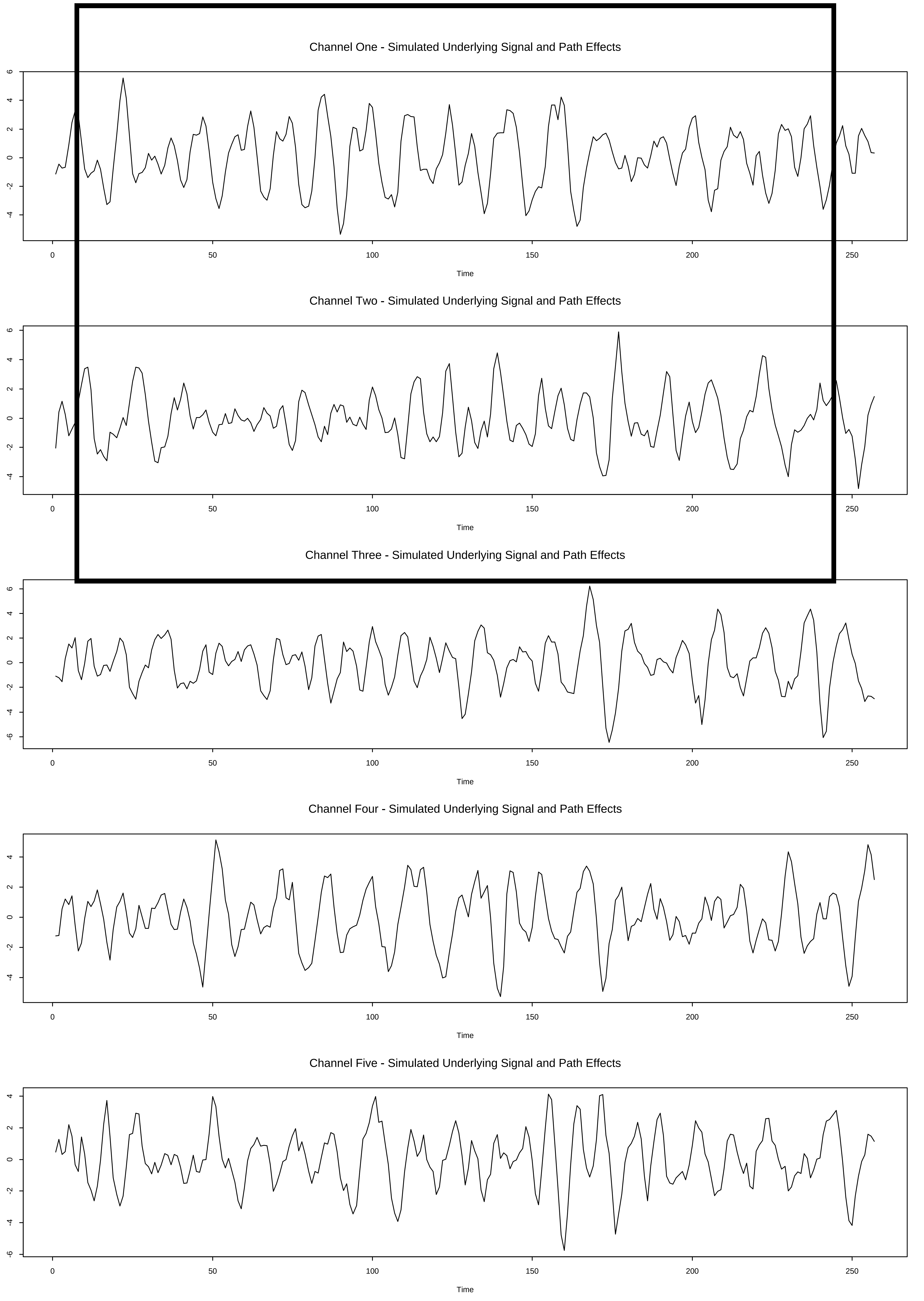

Figure 11: Filtered simulated underlying signals.

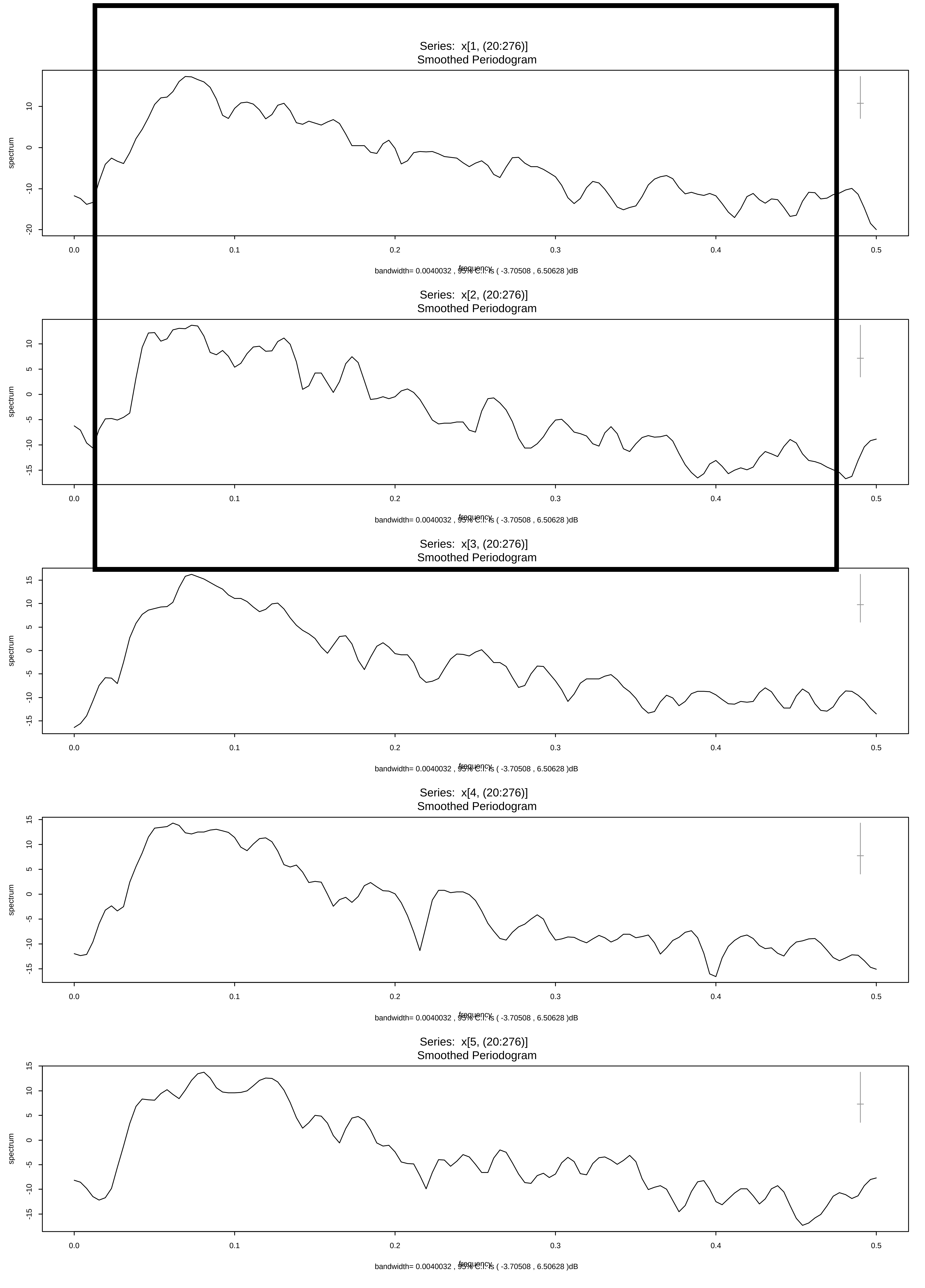

Figure 12: Spectra of the filtered simulated underlying signals.

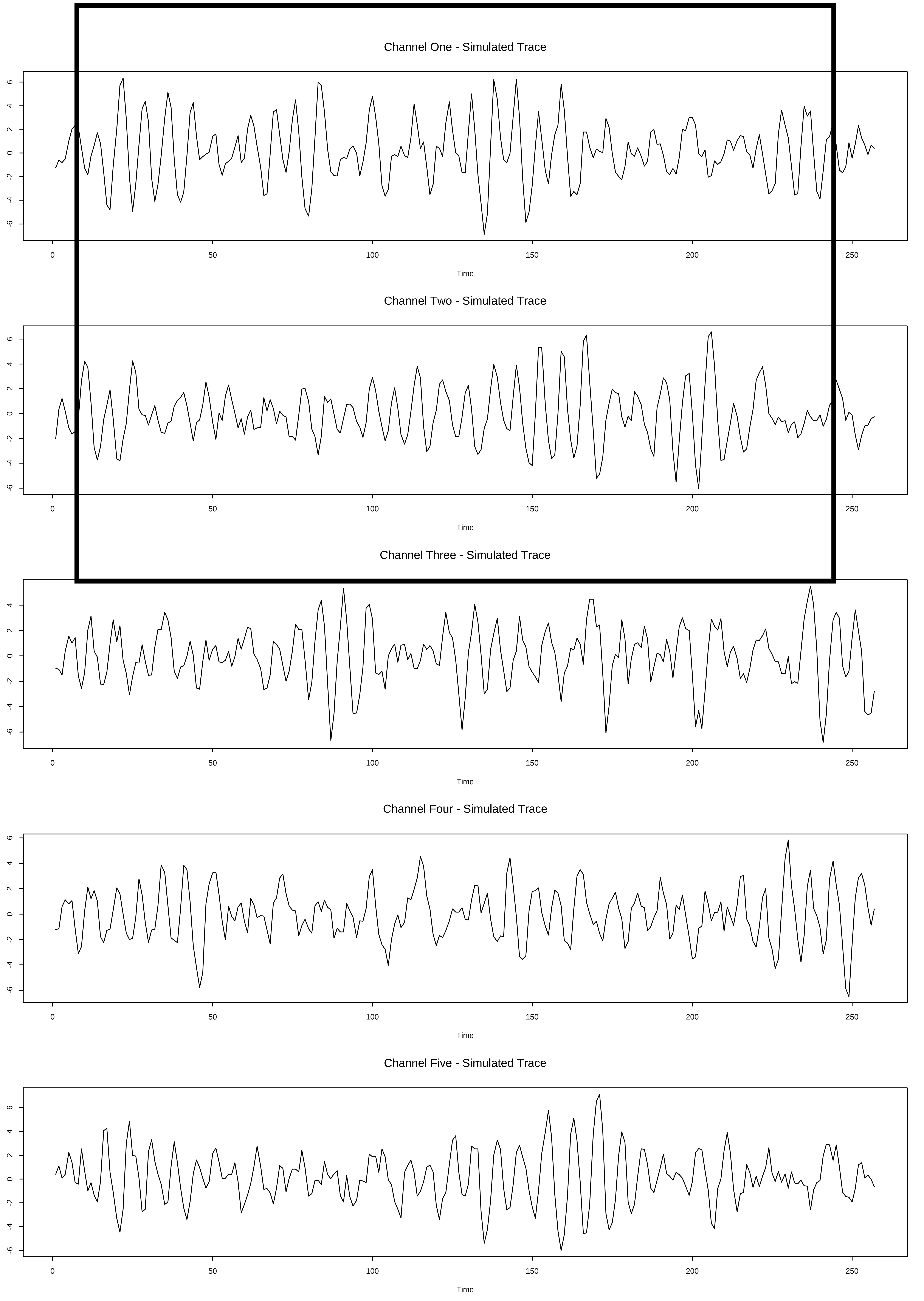

Figure 13: Simulated ripple-fired data traces, using the filtered signals. Note these series do not contain obvious low frequencies.

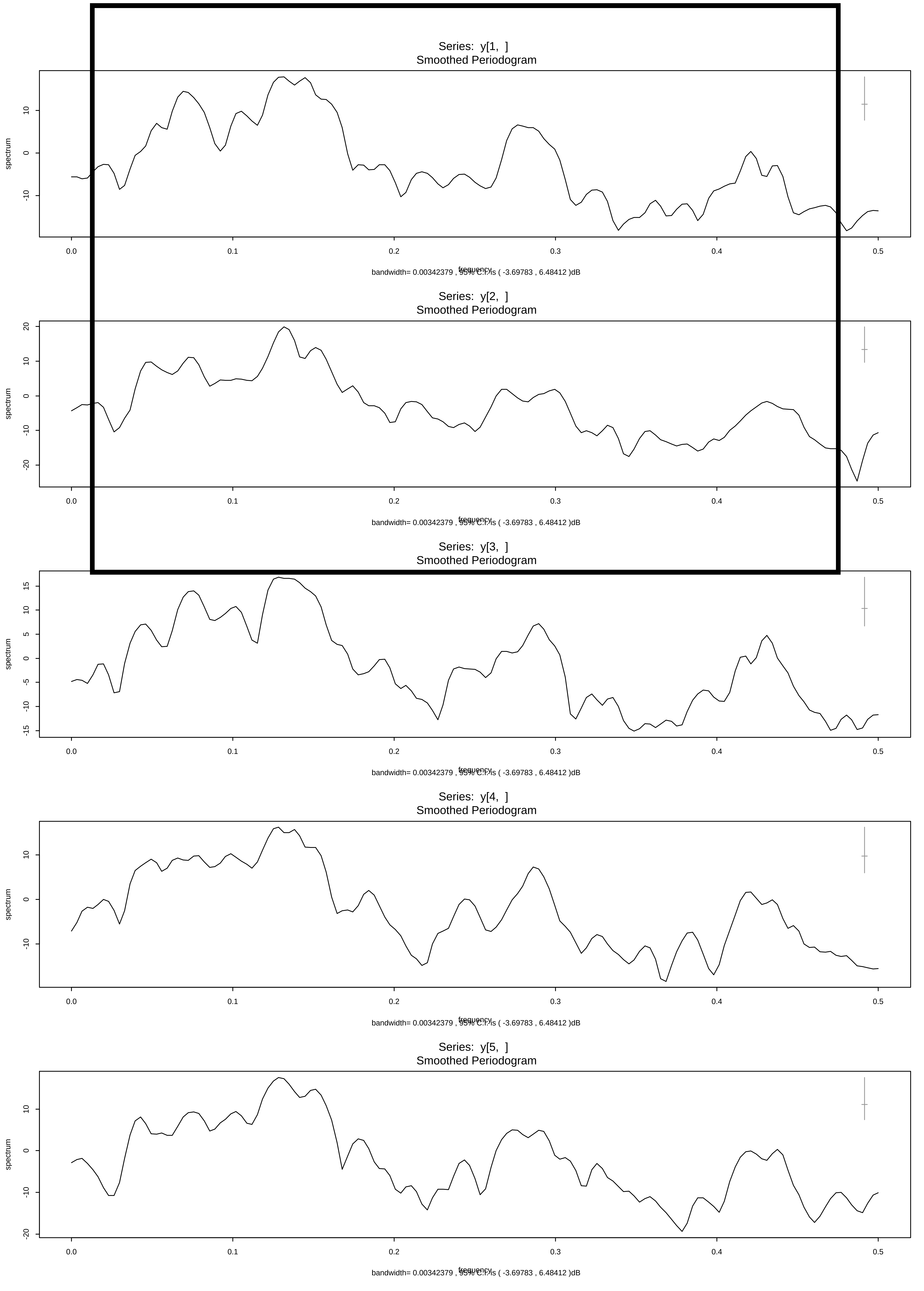

Figure 14: Spectra of the simulated ripple-fired data traces. Note the modulation in the spectra.

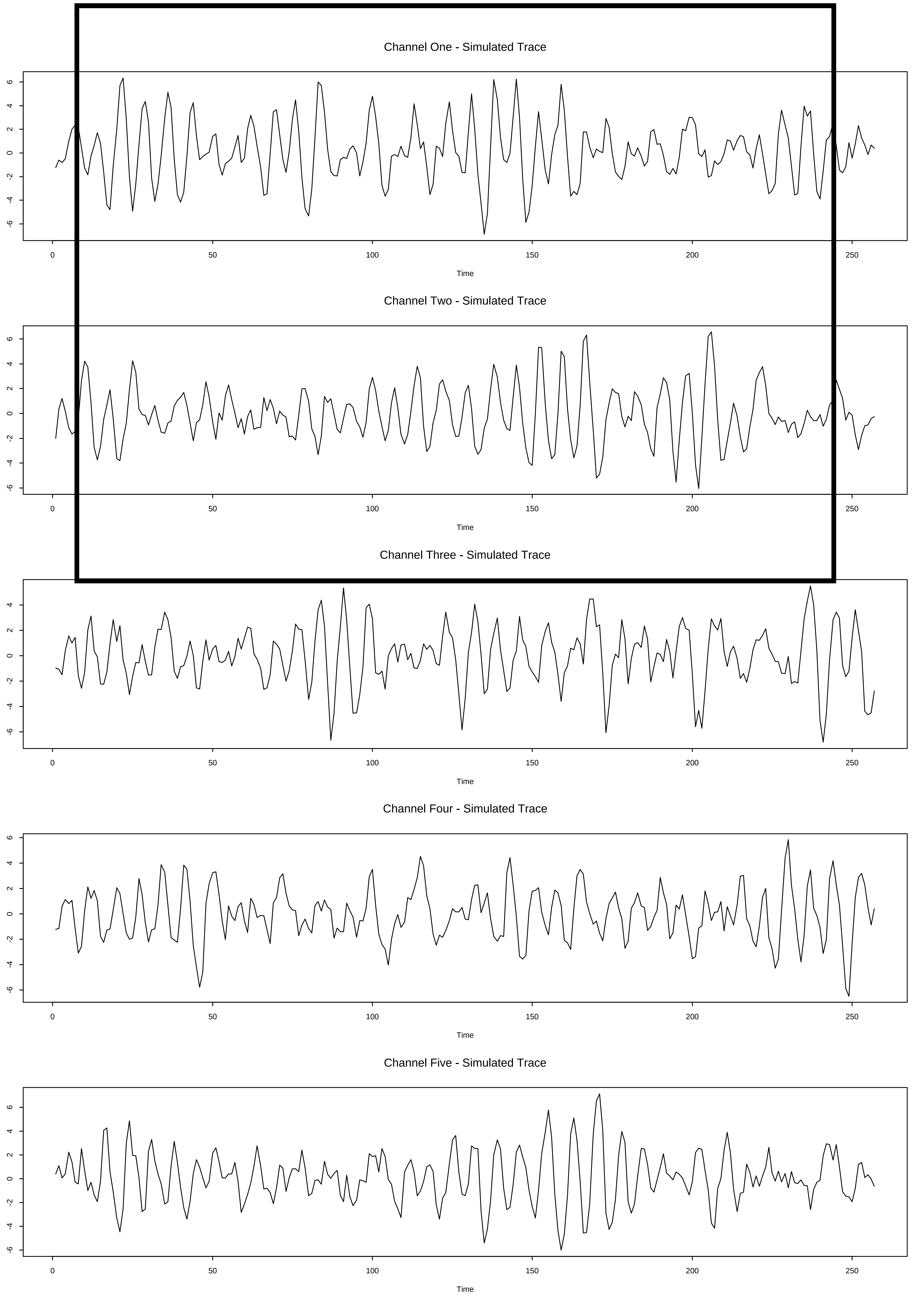

Figure 15: Simulated array data $\mathbf{y}_k$, $k = 1, ..., q$.

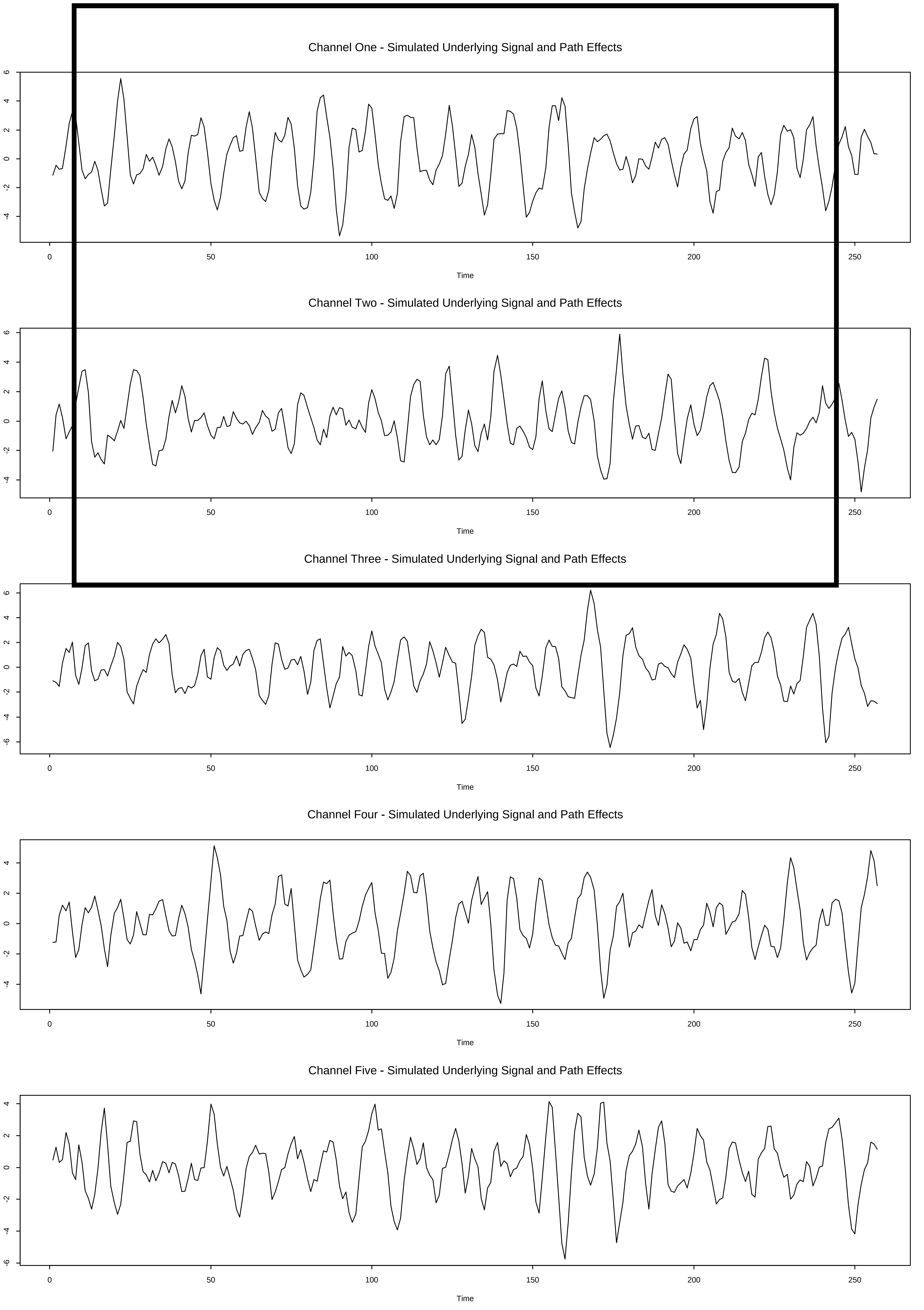

Figure 16: Simulated *underlying signal-path effects* $\mathbf{s}_k$, $k = 1, ..., q$.

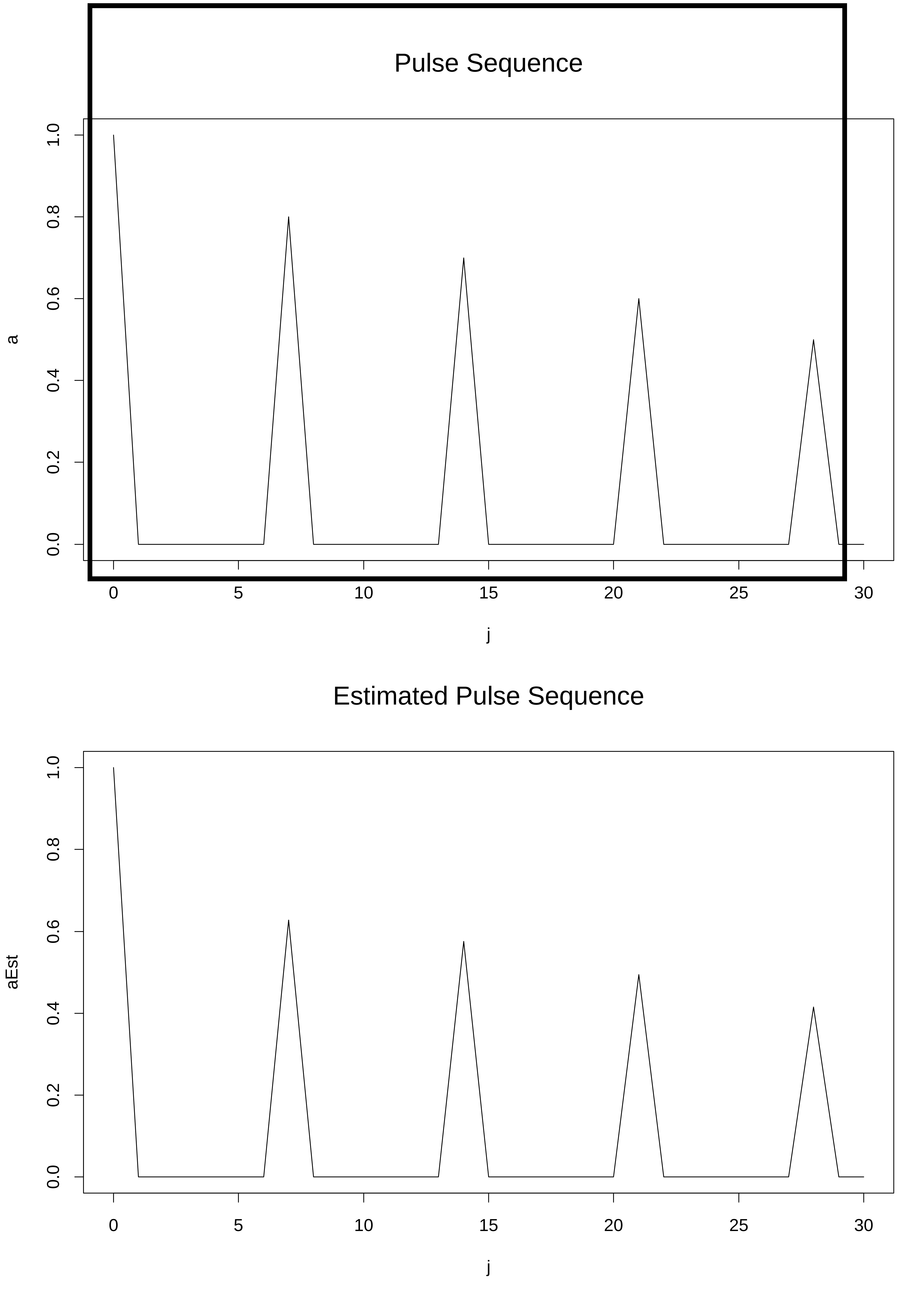

Figure 17: Top: True *pulse sequence*, **a**. Bottom: Estimates.

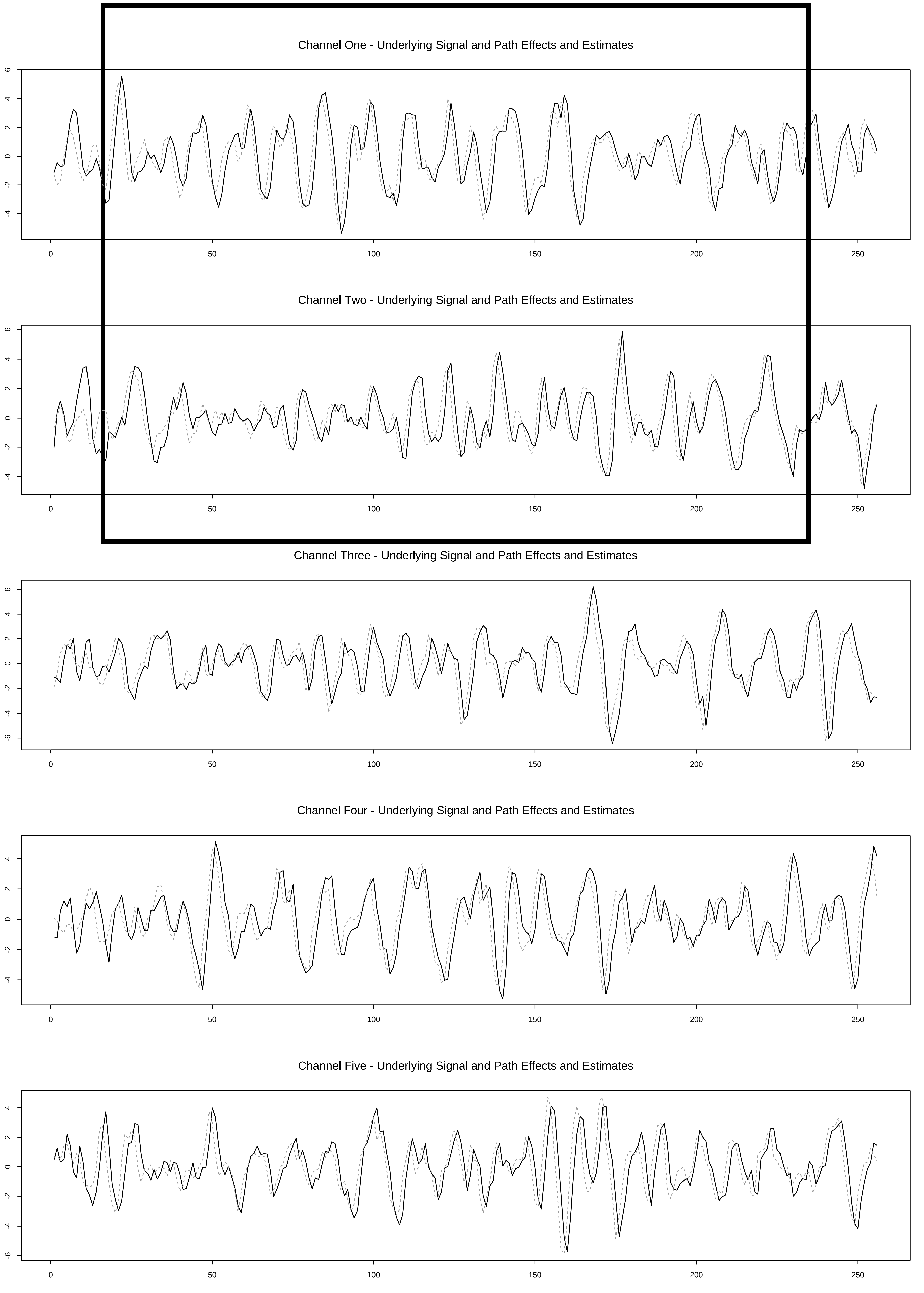

Figure 18: Solid: Simulated *underlying signals-path effects sequence* $\mathbf{s}_k$, $k = 1, .., q$. Dots: Estimates $\hat{\mathbf{s}}_k$ shifted one point to the left.

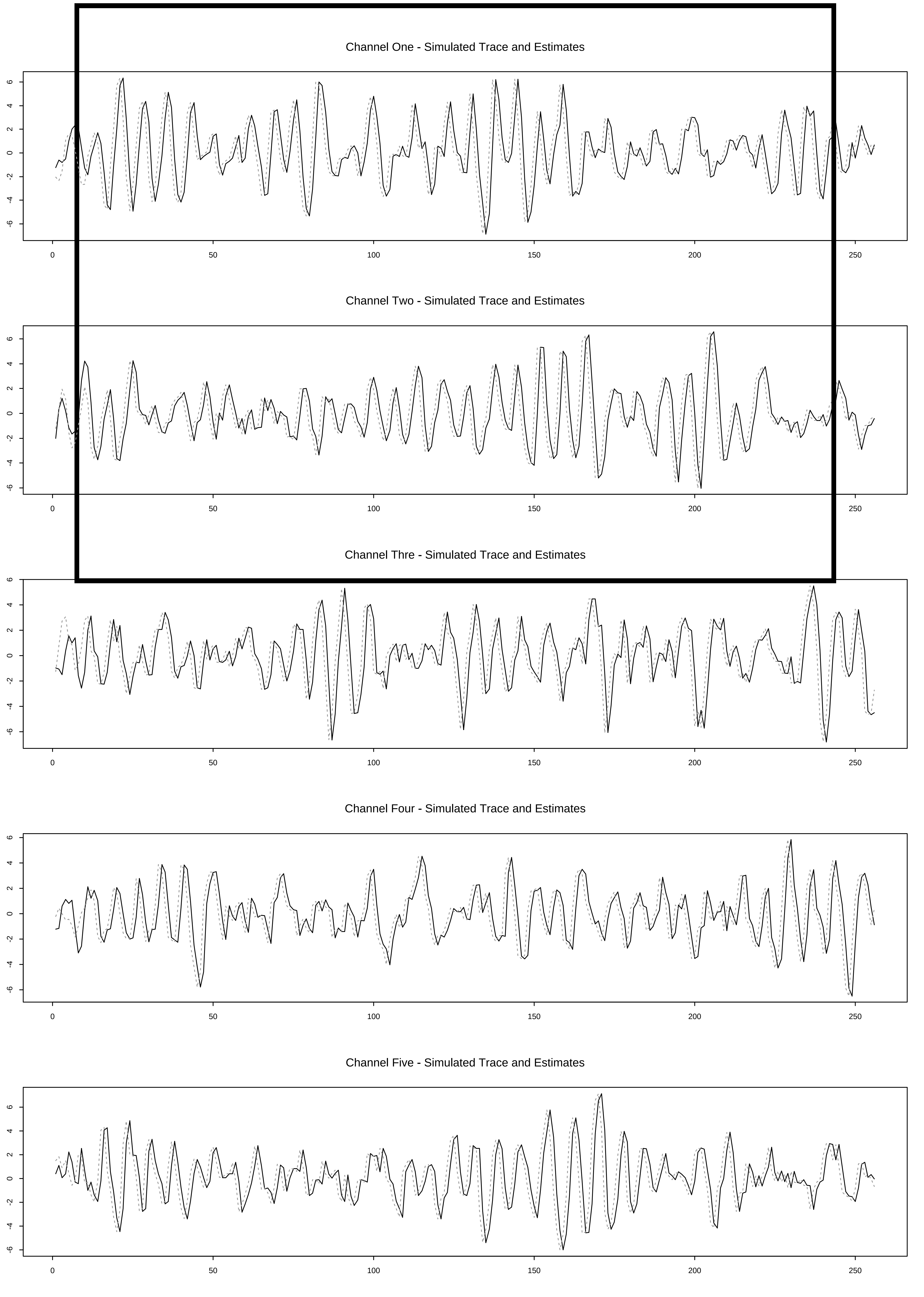

Figure 19: Solid: Simulated trace $\mathbf{y}_k$, $k = 1, ..., q$. Dots: Estimates, $\hat{\mathbf{y}}_k$, shifted one point to the left.

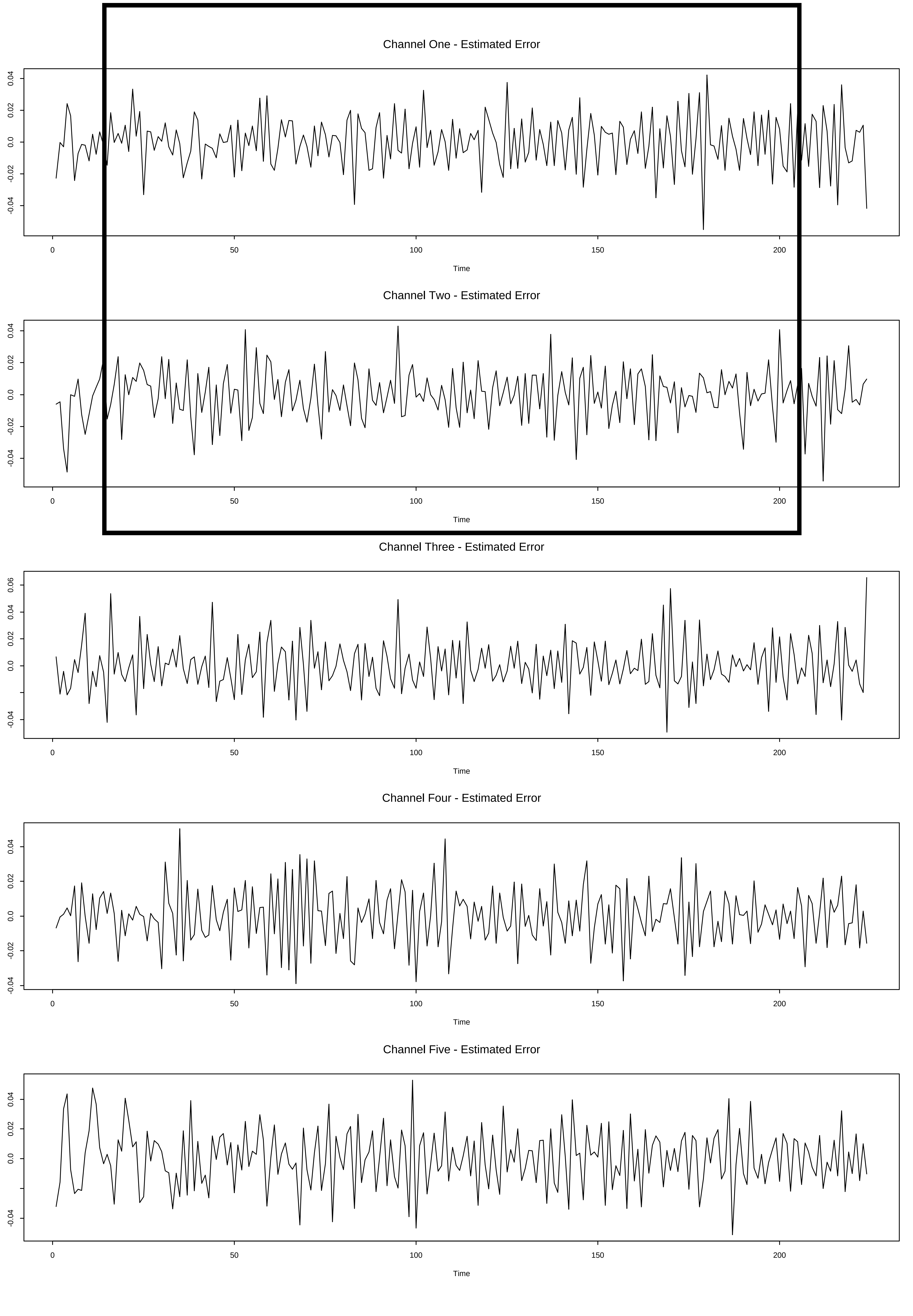

Figure 20: Estimated additive noise on each channel, $\varepsilon_k(t)$, $t = (m-m), ..., (n-m)$.

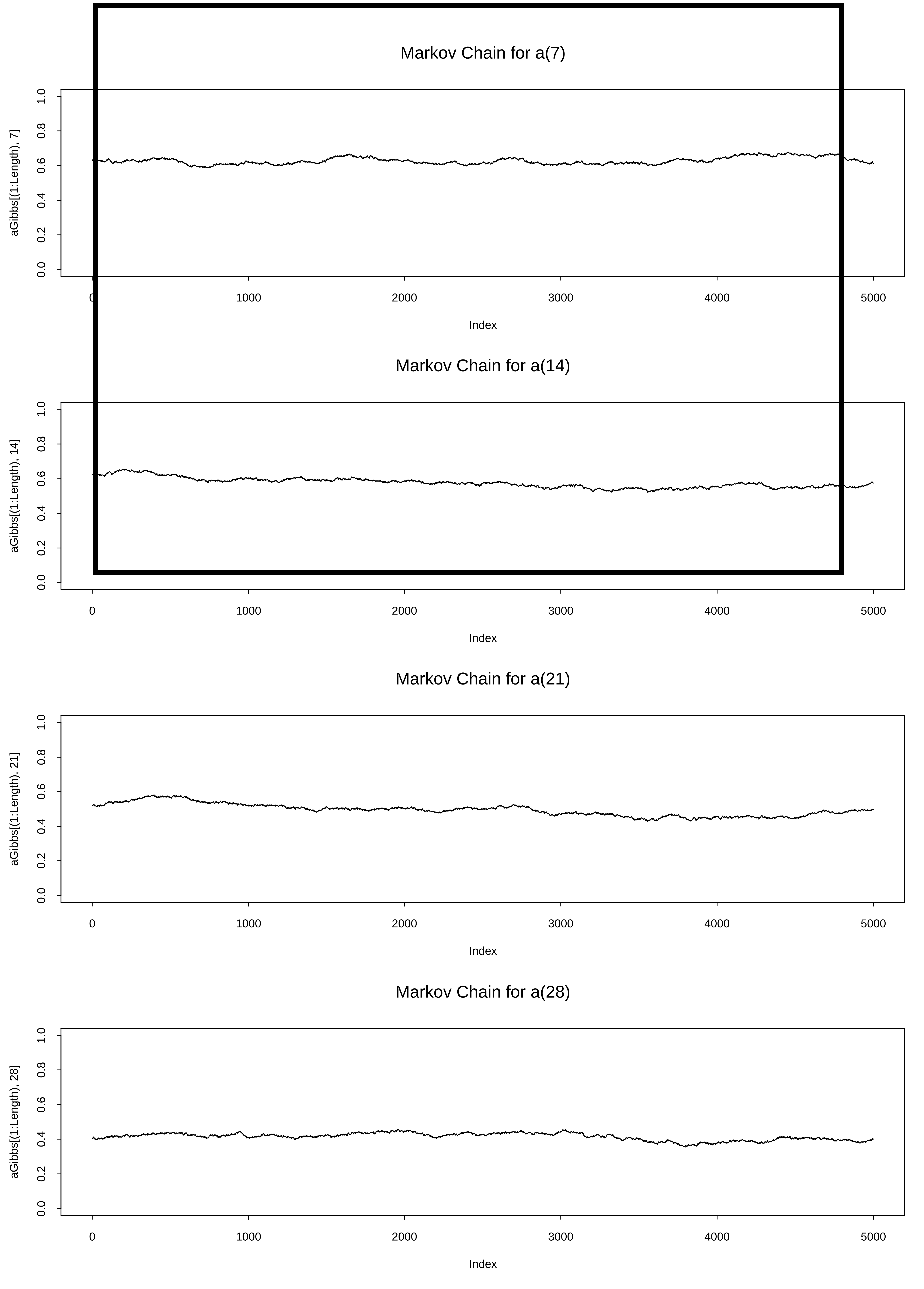

Figure 21: Last 5,000 iterations in the Markov chains produced for a_7, a_{14}, a_{21}, and a_{28}.

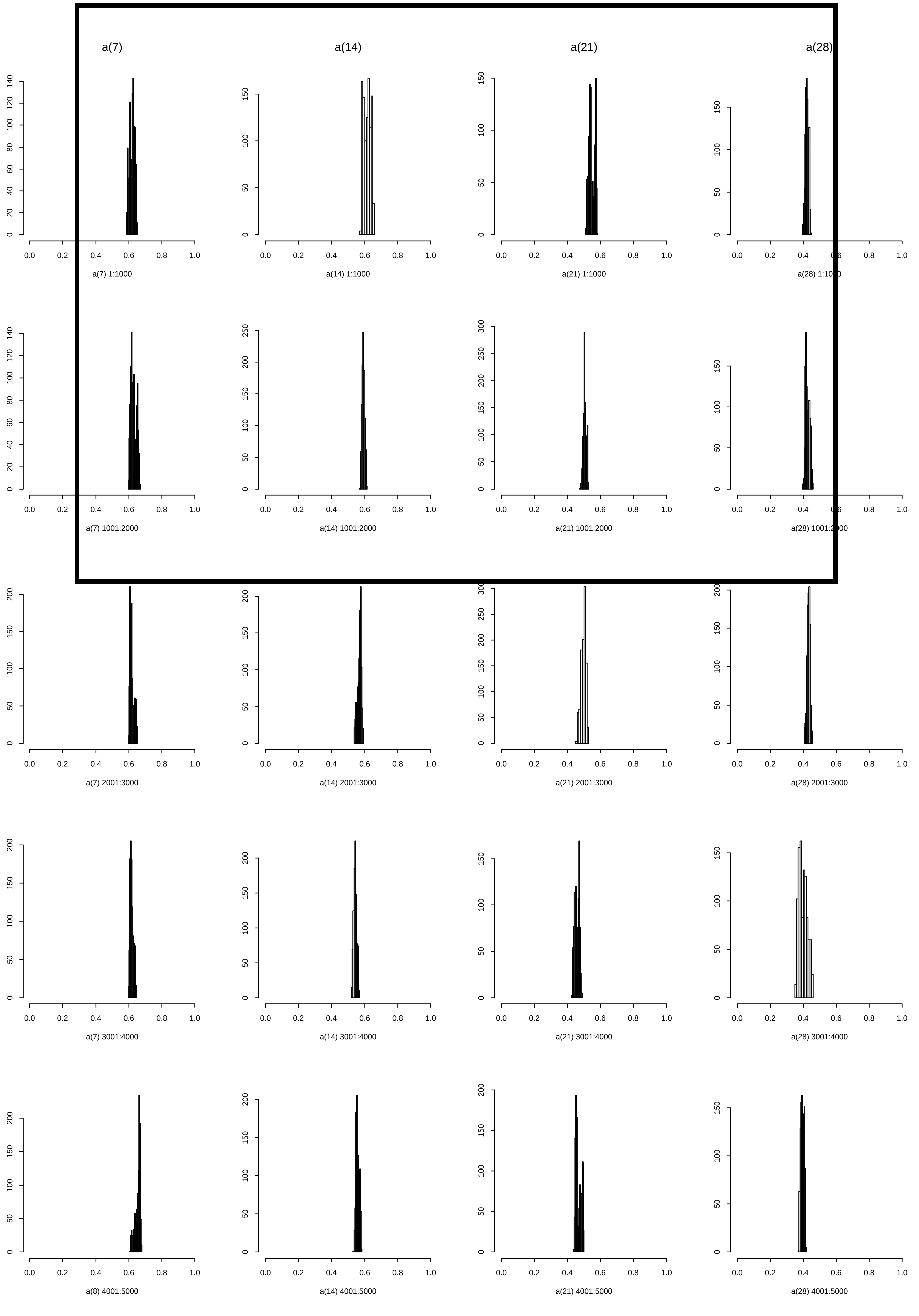

Figure 22: Histograms of every 1,000 iterations, after "burn in," for the nonzero values of **a**. The columns show the stability of the Markov chains for a_7, a_{14}, a_{21}, and a_{28}.

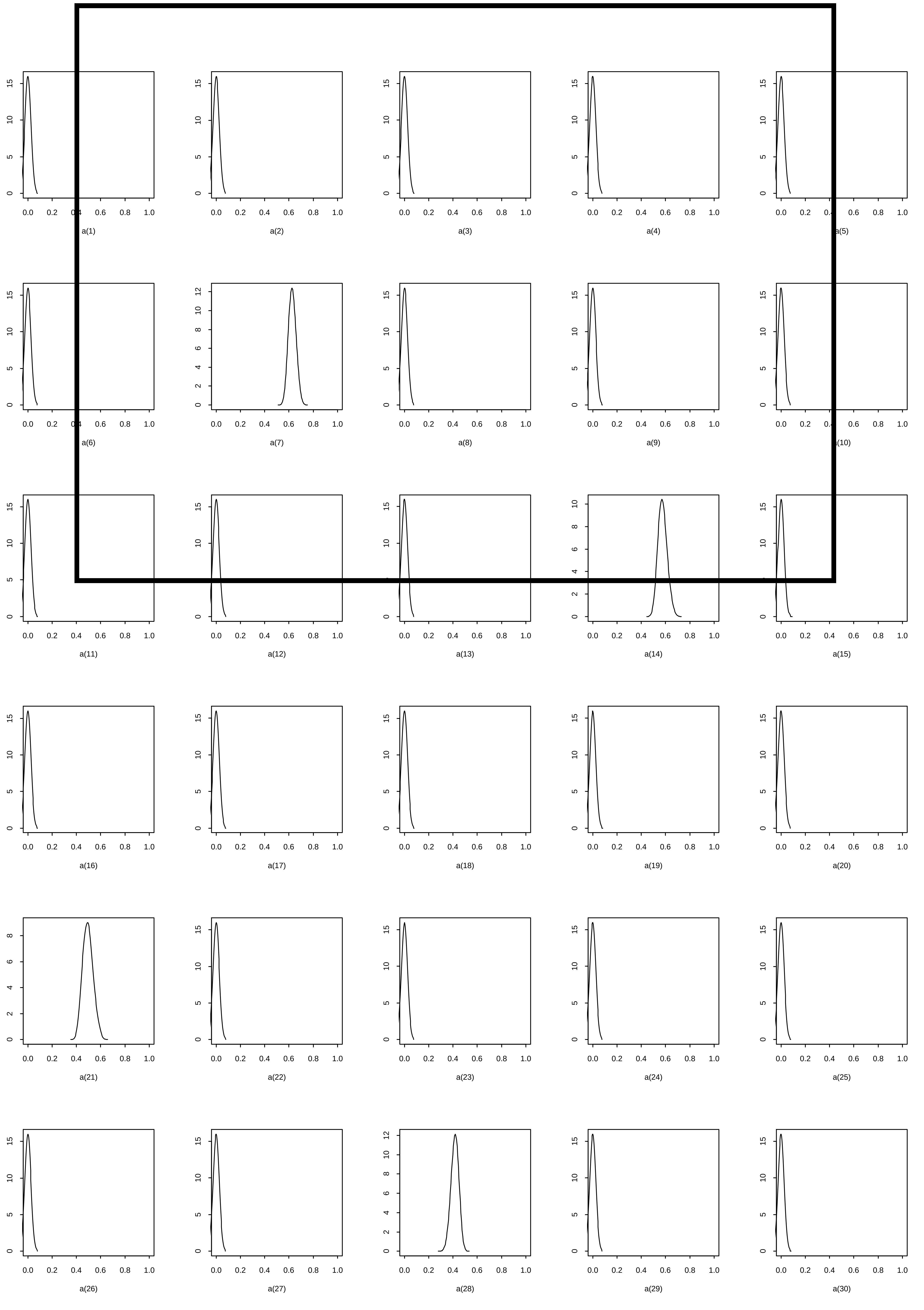

Figure 23: Posteriors of a_j, $j = 1, ..., m$.

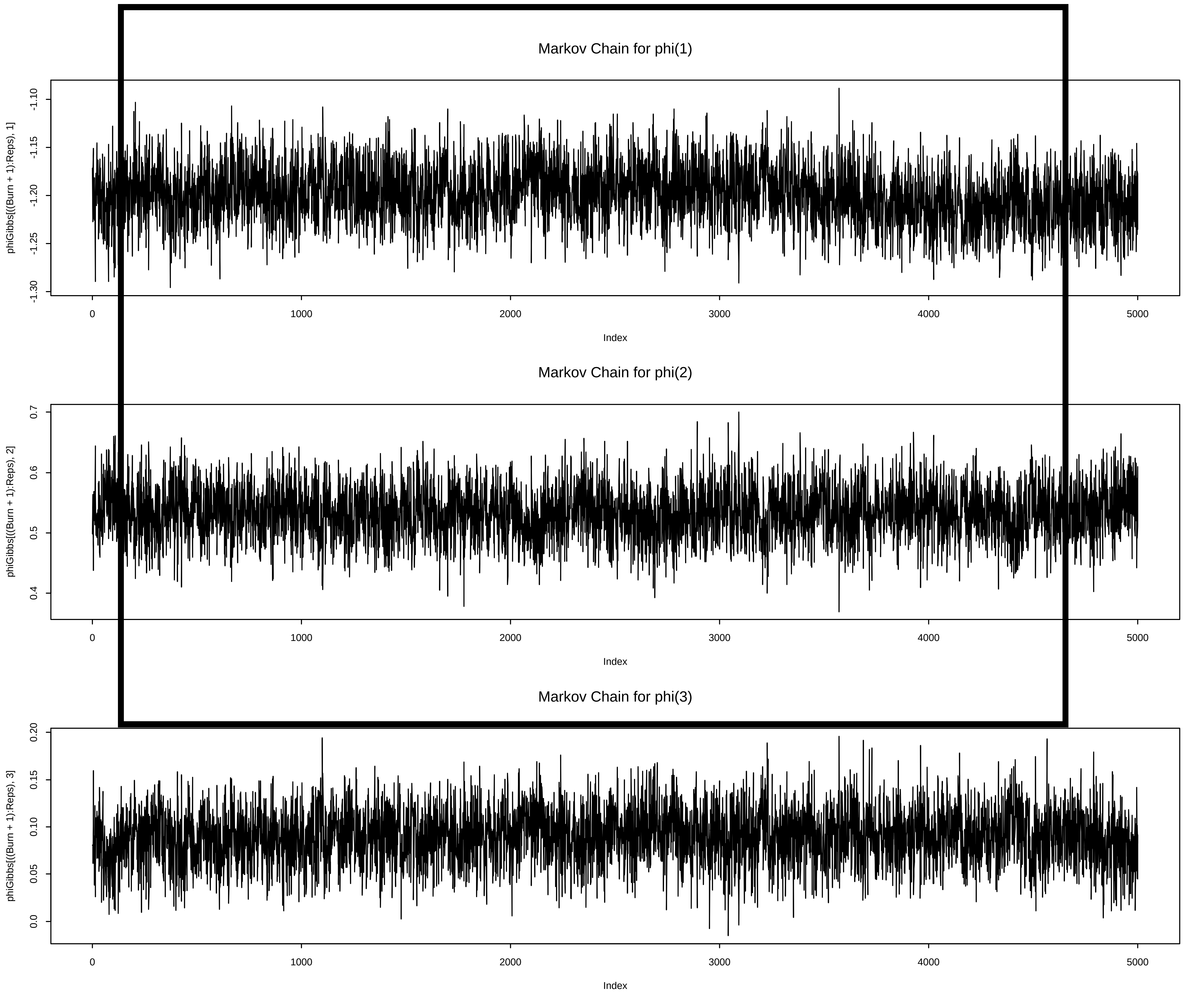

Figure 24: Last 5,000 iterations in the Markov chain produced for ϕ_1, ϕ_2, and ϕ_3.

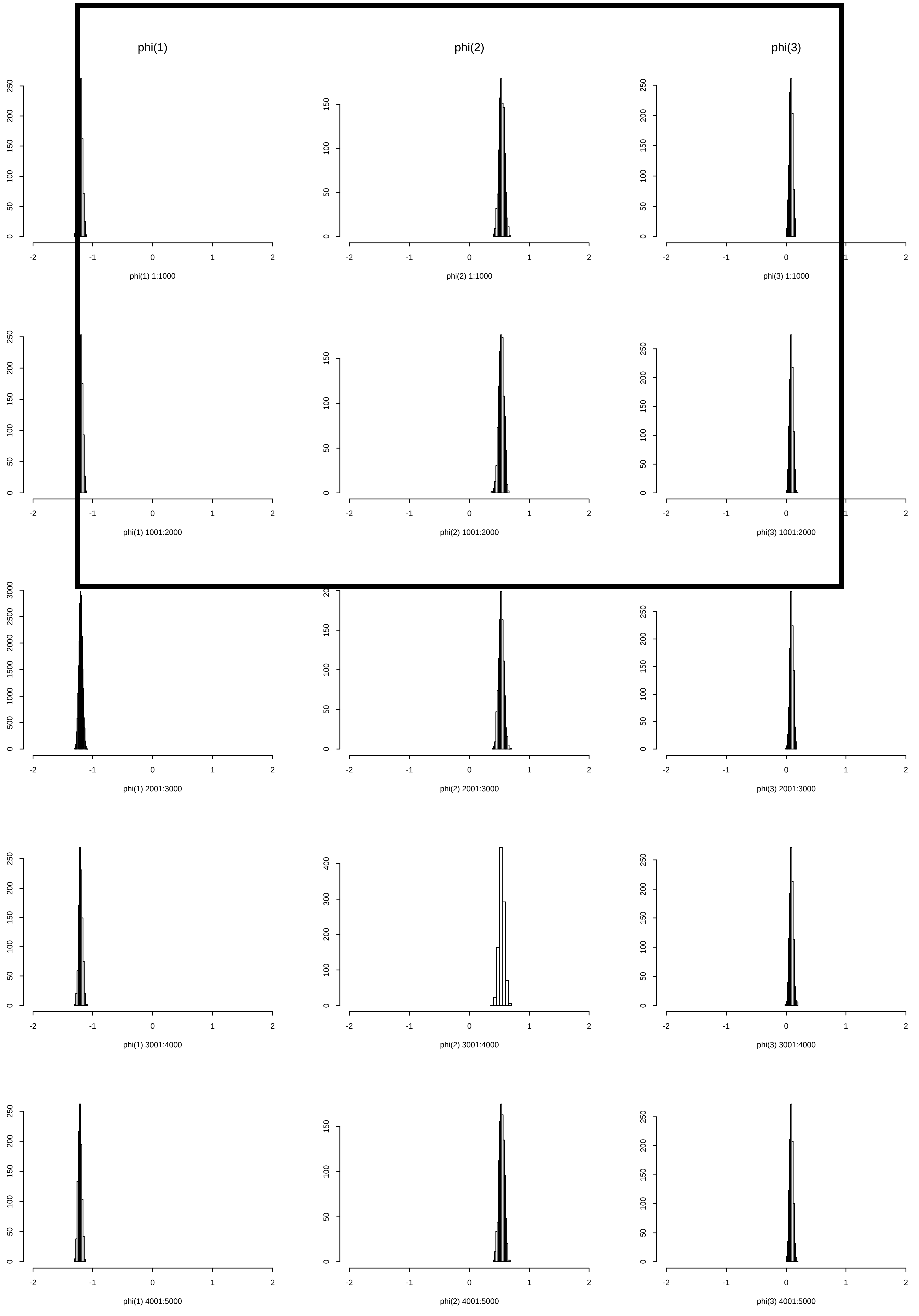

Figure 25: Histograms of every 1,000 iterations, after "burn in," for $\boldsymbol{\phi}$. The columns show the stability of the Markov chains for ϕ_1, ϕ_2, and ϕ_3.

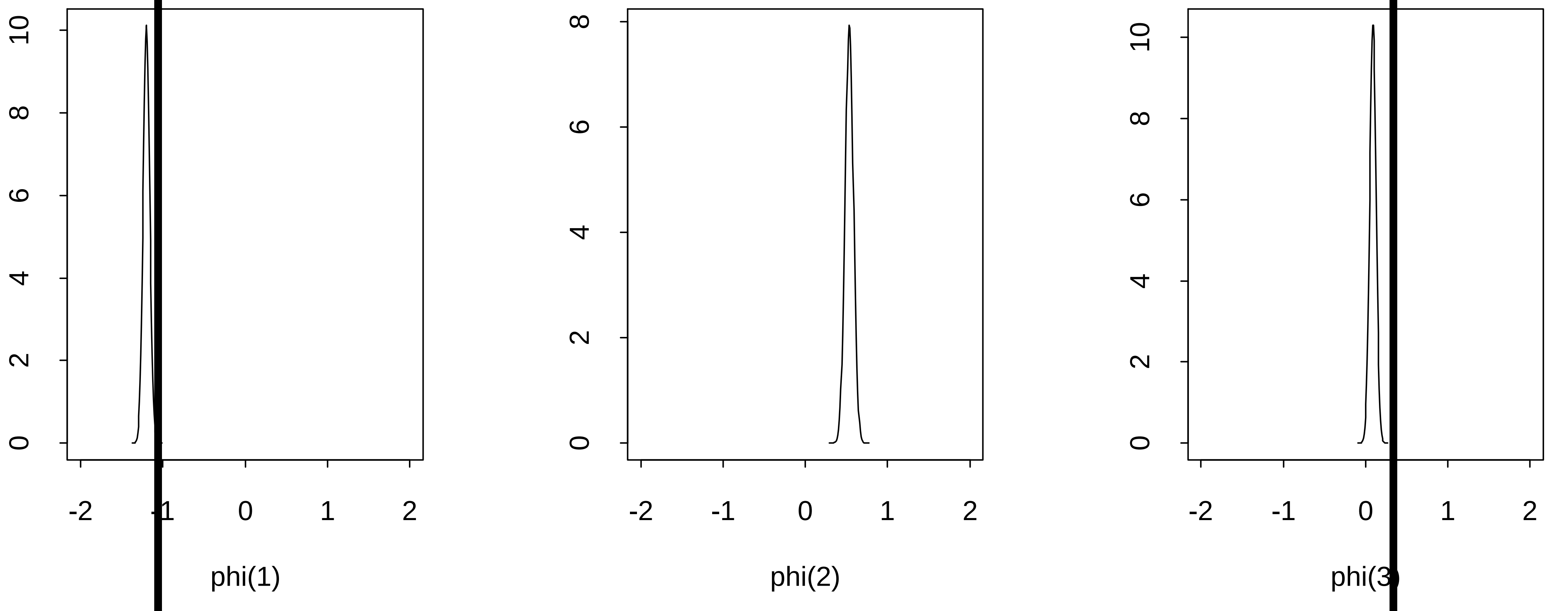

Figure 26: Posterior of ϕ_1, ϕ_2, and ϕ_3.

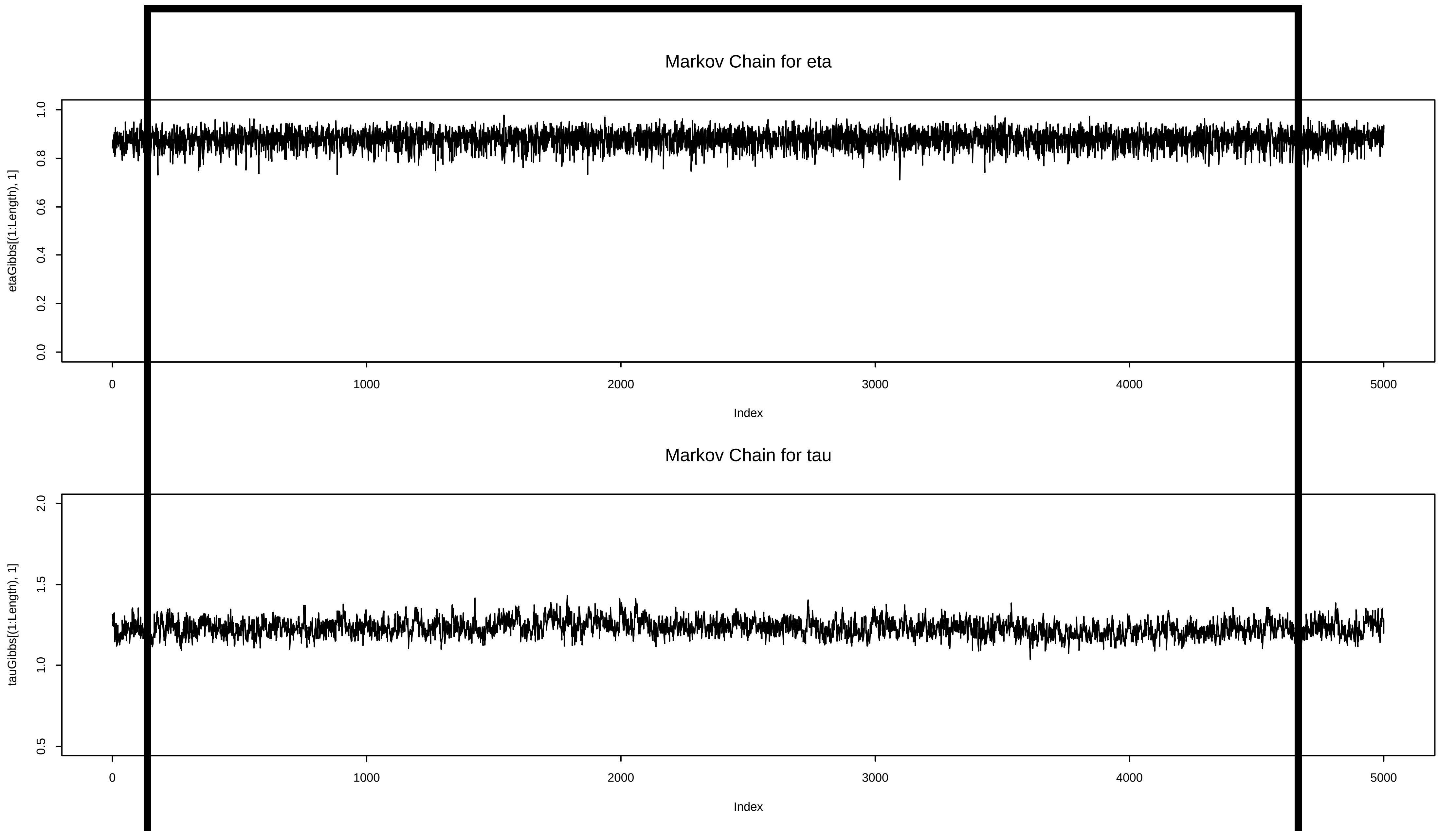

Figure 27. Last 5,000 iterations of the Markov chains for η and τ.

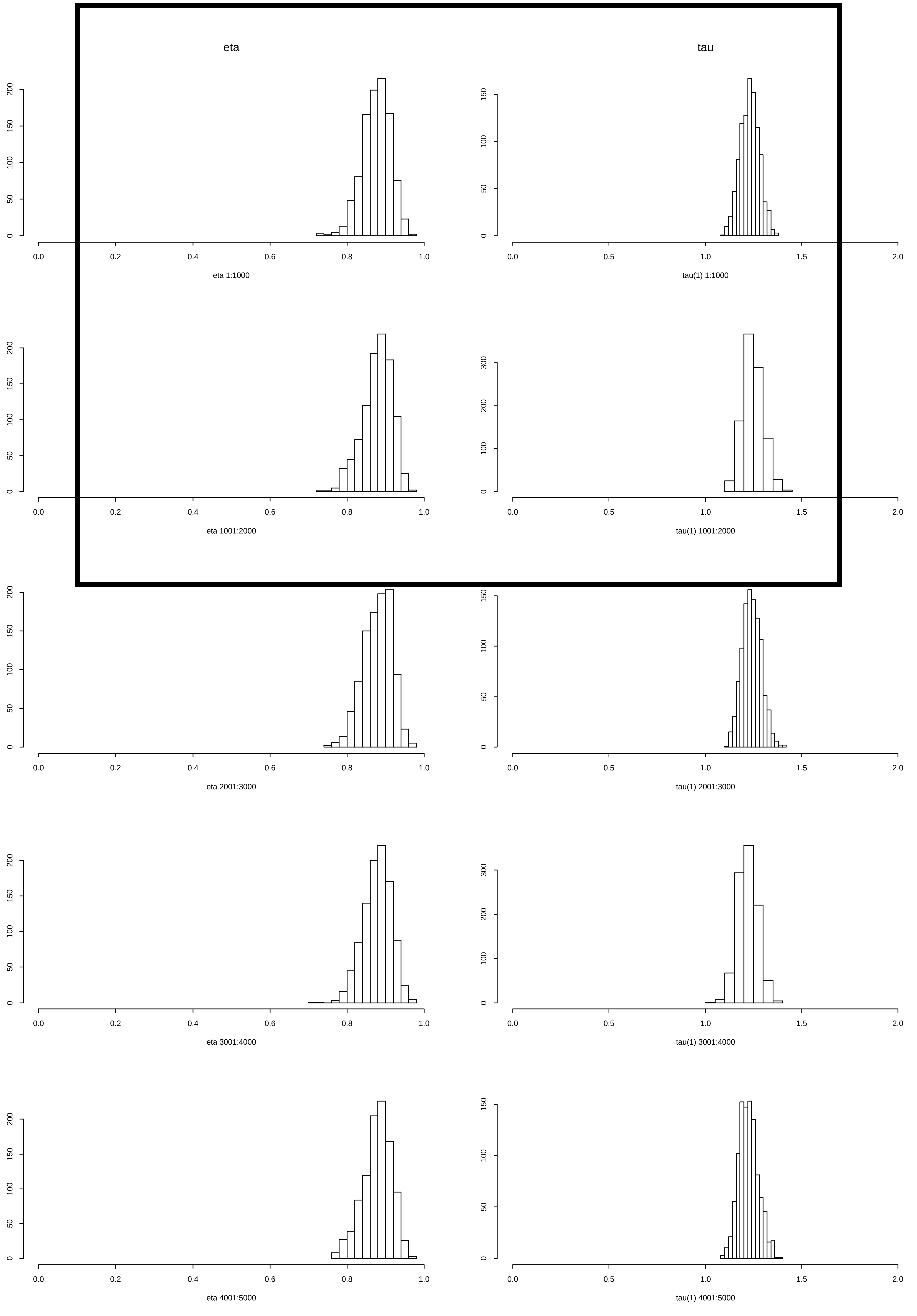

Figure 28: Histograms of every 1,000 iterations, after "burn in," for η and τ.

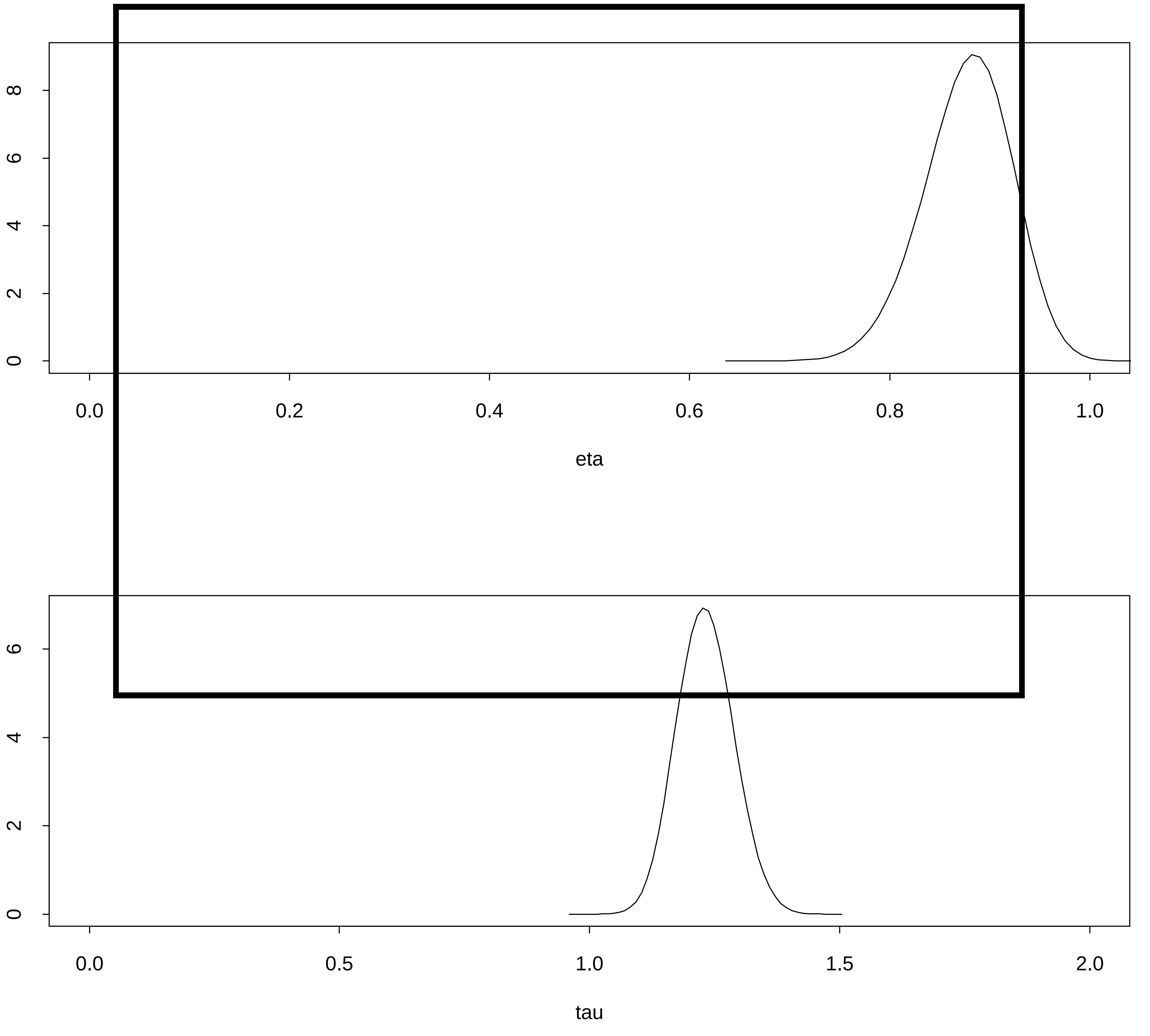

Figure 29: Posteriors of η and τ.

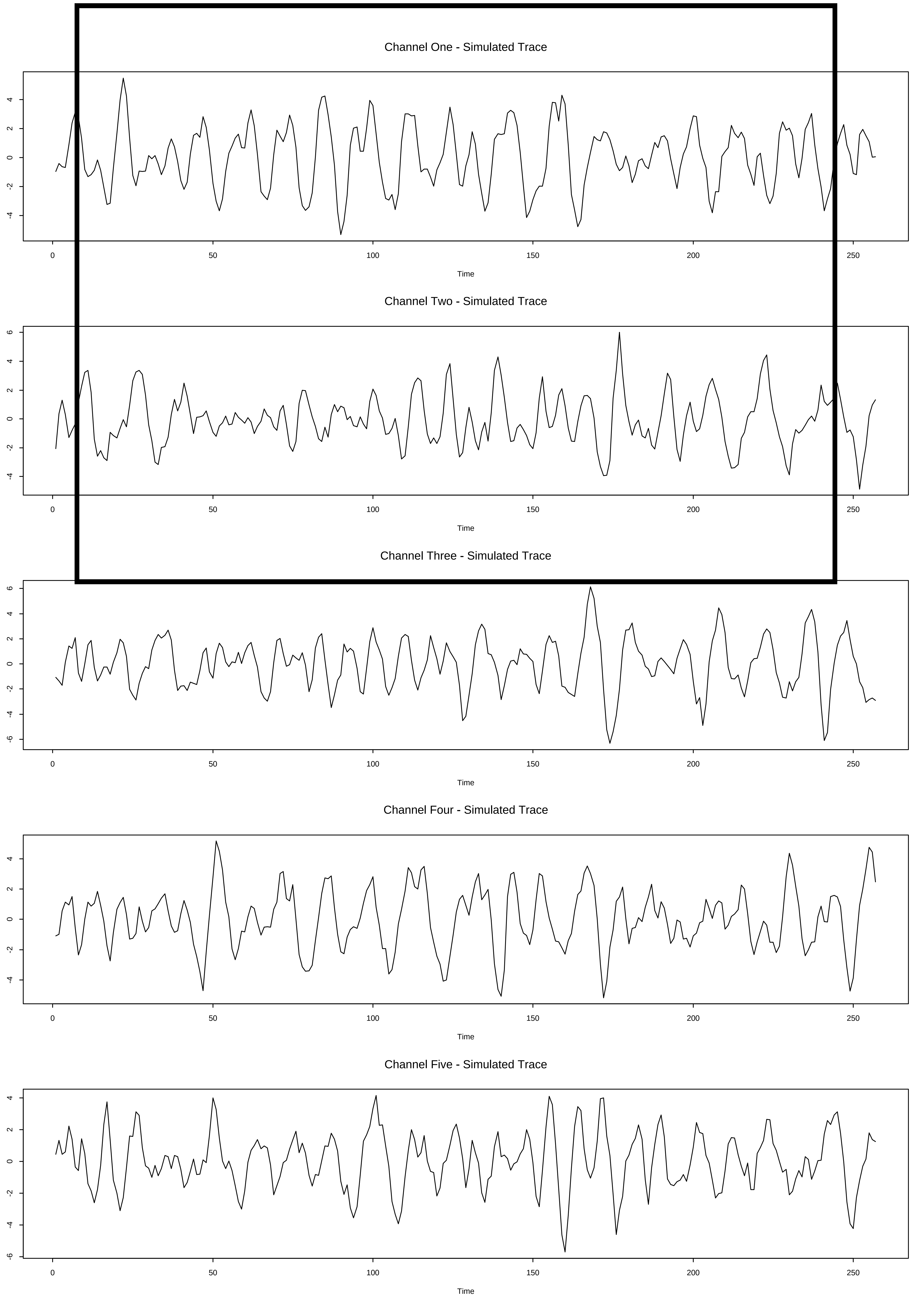

Figure 30: Simulated data with no delayed signals.

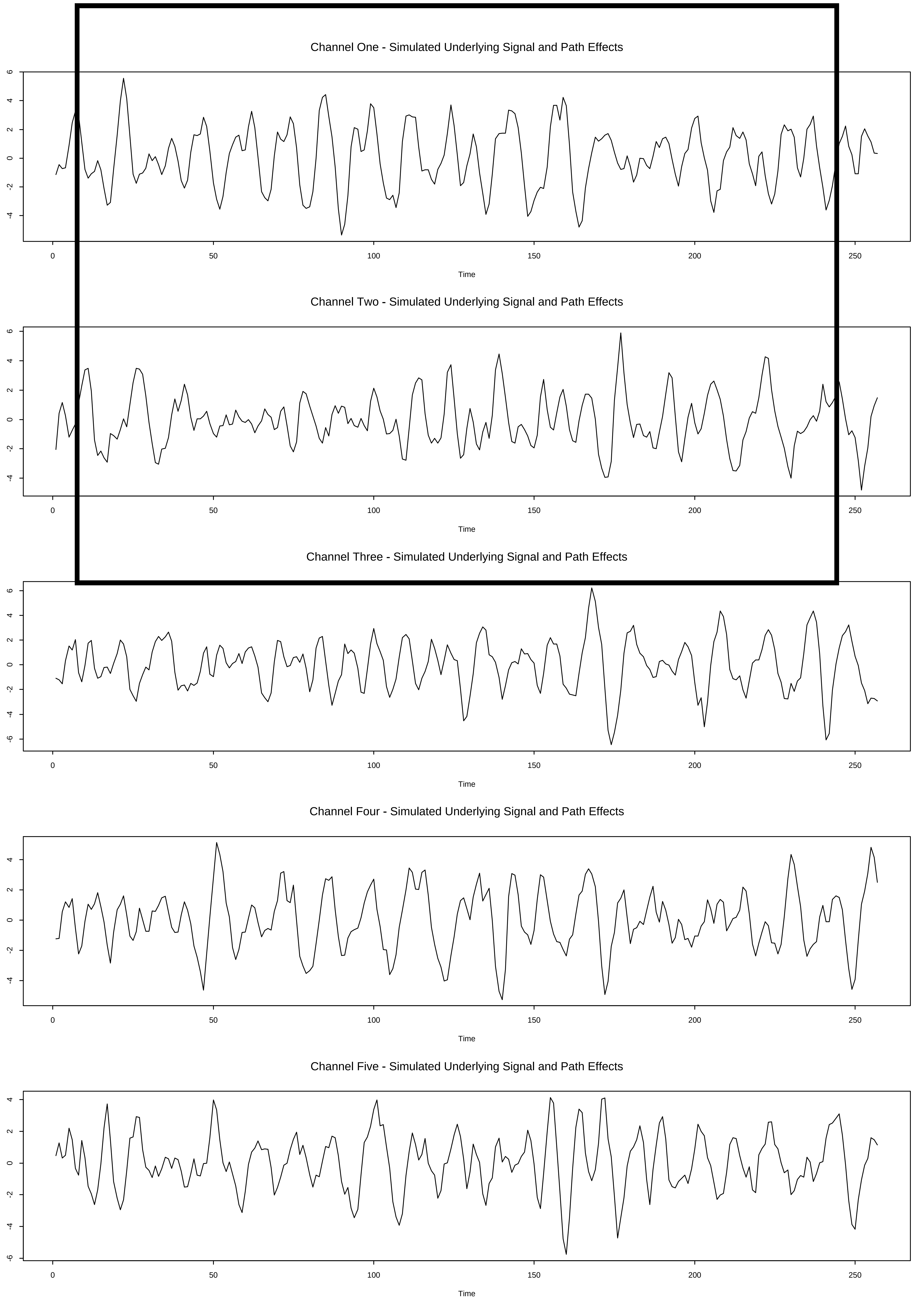

Figure 31: Simulated underlying signal.

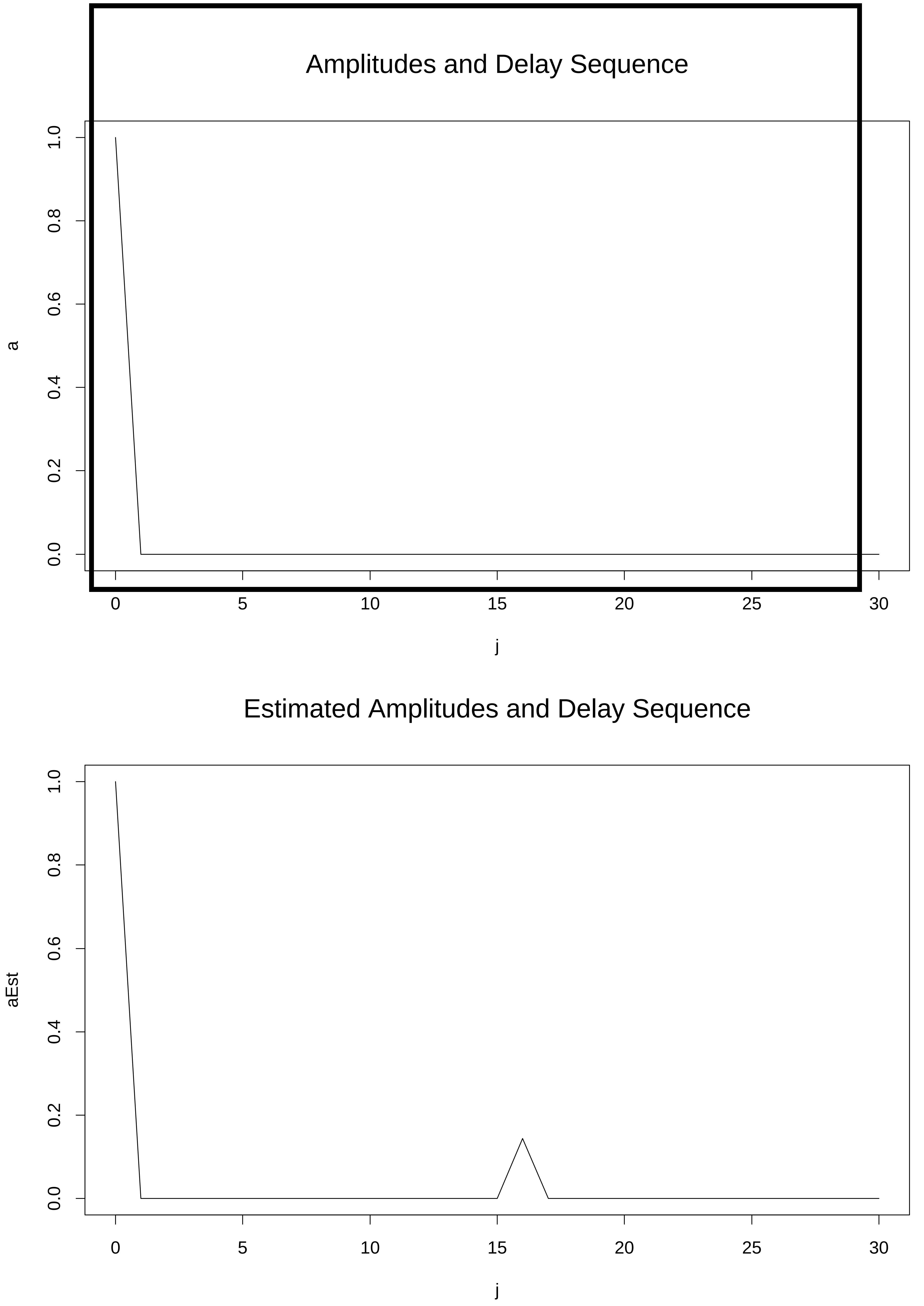

Figure 32: Top: “True” *pulse sequence*, **a**, containing no delays. Bottom: Estimates.